Chapter 13
Electrochemically Fabricated Microelectromechanical Systems/ Nanoelectromechanical Systems (MEMS/NEMS)

Carlos M. Hangarter, Thomas George, and Nosang V. Myung

13.1 Introduction

Microelectromechanical Systems (MEMS) [1] and its more recent extension Nanoelectromechanical Systems (NEMS) [2] are successful offshoots of the semiconductor revolution, which was the hallmark of the latter half of the previous century [3]. Both MEMS and NEMS have established themselves as successful fields of endeavor in their own right. In fact, it is fair to say that all nonintegrated circuit (IC) technologies are included under the MEMS/NEMS umbrella. Although the vast majority of MEMS/NEMS technologies deal with the design and fabrication of novel sensors and actuators [3], ancillary technologies such as interconnects and packaging form an important part of MEMS and NEMS [4]. In many cases, MEMS/NEMS also find applications, not as stand-alone devices but as the key enabling subcomponents of otherwise conventionally fabricated systems [2]. This chapter will provide a survey of MEMS/NEMS fabrication and device technologies with particular emphasis on electrochemistry- based fabrication techniques and novel devices/instruments technologies that can be developed using electrochemistry.

13.2 Electrochemical Fabrication Techniques in MEMS/NEMS

Electrochemical fabrication techniques offer tremendous versatility as cost-effective methods to generate MEMS/NEMS materials and structures. The batch processing nature of these methods carried out at near room temperature in ambient pressure,

C.M. Hangarter and N.V. Myung (✉)
Department of Chemical and Environmental Engineering,
University of California-Riverside, Riverside, CA, 92521, USA
e-mail: myung@engr.ucr.edu

T. George
ViaLogy Corporation, Altadena, CA, 91001, USA

T. Osaka et al. (eds.), *Electrochemical Nanotechnologies,*
Nanostructure Science and Technology, DOI 10.1007/978-1-4419-1424-8_13,

also allows for easy integration into Integrated Circuit (IC) and MEMS manufacturing technology. However, to date, the diverse capabilities of electrochemical processes have been largely under-utilized in the creation of novel MEMS/NEMS devices. Fabrication is still dominated by vacuum processes and silicon technology, not only because silicon has been so well characterized in terms of processing and as a material, being continually fueled by the semiconductor industry, but also because silicon is inherently predictable. By comparison, electrochemically fabricated materials have lagged, with more recent thrusts to correlate deposition conditions to crystalline structure and material properties. Structural properties of electroformed materials, such as film stress, adhesion, and elastic modulus, are further complicated as they depend not only on deposition parameters but also on previous and subsequent deposits [5]. This gap between synthesis and properties is also due to the complexity of electrochemical processes. While an electrolytic solution with an applied electric current as a reducing or oxidizing medium is simple in theory, electrochemical systems can become complicated with a potentially active carrier phase, current distribution effects, functional additives, and mass transfer phenomena. With the exception of electroless deposition, these systems are controlled by both mass transport and current distribution phenomena [6], which, though outside the scope of this chapter, are critical for implementing electrochemical microfabrication of MEMS and NEMS. In the MEMS/NEMS context, electrochemistry has nevertheless made significant progress, functioning as an important tool for deposition, removal, and surface modification of microstructures described herein.

13.2.1 Electrodeposition

Simply stated, electrodeposition, also known as electroplating, is the use of electric current to deposit metal ions from a liquid solution onto a surface. More specifically, aqueous, organic, and ionic solutions can be used as the electrolyte for electrodeposition with the latter two being restricted primarily by cost and safety considerations. The substrate must also be conductive; a limitation that often necessitates physical deposition as an alternate fabrication technique, especially for dielectric materials. Nevertheless, electrodeposition has proven particularly robust, as a "workhorse" electrochemical technique for MEMS fabrication. Electrodeposition is particularly cost effective for producing thick films (tens of microns to millimeters), which is not practical using vacuum deposition processes. Electrodeposited films also conform extremely well to the surface topography, filling recesses and covering complex geometries that are not covered easily with line-of-sight physically deposited coatings. In addition, the crystallographic structure and orientation can be controlled for desired material properties through adjustments to the solution composition, deposition conditions, and the type and amount of additives and complex agents [7]. Electrodeposition is also a powerful tool for alloying,

being able to deposit a wide range of solid solutions and nonstoichiometric alloys that are not attainable with other methods. Recent advances in electrodeposition for MEMS have focused on deposition optimization for copper interconnects, magnetic media storage devices, and magnetically-actuated MEMS with particular interest in tuning physical properties including magnetic properties, elastic properties, and microstructure.

Since 1997 the damascene copper electroplating process has been utilized in silicon chip manufacturing for "super-conformal" plating of holes and trenches. This market has revitalized copper plating research, focusing on the influence of additives, and elucidating their roles as suppressors, levelers, and accelerators [8, 9]. In the magnetic storage industry, soft magnetic materials have gained considerable attention for their use as recording heads. These materials, also commonly used for magnetic-MEMS, require excellent magnetic properties, (high magnetic saturation, low coercivity, high permeability, and zero magnetostriction), good adhesion, low-stress, low electrical resistance, good thermal stability, and high corrosion resistance [10]. These specifications are more demanding for electroplated materials, which are vulnerable to corrosion due to anodic surface activation by organic additives [10]. To meet these requirements, investigators have turned to ternary and quaternary alloys of CoNi and CoFe for their enhanced magnetic properties with uncompromised mechanical properties [11]. Although hard magnetic materials have not been typically used in magnetic-MEMS, they have several advantages for magnetic actuation, including low power requirements, high remanence, and high coercivity, which have motivated investigators to develop new electrodeposition processes for these materials. Many of these permanent or hard magnetic materials are Co-based with the inclusion of a nonmagnetic material, typically P, to increase coercivity [10, 12].

13.2.2 Electroless Deposition

Electroless deposition is an autocatalytic reaction utilizing a chemical reducing agent (e.g. sodium hypophosphite, amineboranes, hydrazine, or sodium boron hydride) to reduce metal ions onto surfaces. This method can be used to plate insulating materials and fabrics as well as metals; the surface need only be catalytically active to initiate the self propagating process [13]. Nonconducting surfaces can be rendered catalytic by a series of chemical treatments [14]. Film composition and efficiency of these baths can be controlled by electrolyte recipes and operating temperature, typically ranging between 70 and 90°C [14]. The main benefit of electroless deposition is a uniformly thick layer over any profile due to the absence of an electric field [15]. The downside to electroless deposition is the introduction of several modes of stress, which if not mitigated, can lead to fatigue and cracking. The most common type of stress associated with electroless deposition is due to differences in thermal expansion coefficients between the deposited material and the substrate. The resulting stress can be either compressive or tensile

depending on which coefficient is greater [16]. These systems are also prone to voids and significant hydrogen evolution, which can result in tensile stress and hydrogen embrittlement [17].

Currently, electroless materials for MEMS and Ultra Large Scale Integration (ULSI) include Cu, Co, Ni, Ag, and their alloys [18]. The uniform films, nanometer-size crystals, and ability to coat nonconducting materials have allowed the use of electroless deposits for interconnects, barrier layers, packaging, and potential nanoelectronics [19]. In this regard, electroless copper plating has been primarily investigated for IC applications and was utilized in semiconductor manufacturing as the predecessor to the damascene process. Electroless nickel is the other extensively studied material, and is selected primarily for its corrosion resistance and mechanical properties.

13.2.3 Electrochemical Etching

Electrochemical etching is a facile technique for the topographical dissolution of solids with nanometer precision through control of current density or voltage, fluid flow, etching time, and electrolyte composition. Electrochemical etching can also be used to create porous oxides by anodic etching processes or even porous metals by de-alloying, a process by which the less thermodynamically stable or more kinetically active component is preferentially etched away from an alloy [20]. Scanning tunneling microscopy (STM) also relies on electrochemical etching processes in order to synthesize the atomically sharp apex of the tips used in STM instruments, with the ease of fabrication and excellent reproducibility of this method being the key factors leading to its rapid commercialization [21]. For traditional MEMS devices, electrochemical etching serves as an alternative or complementary technique to the popular chemomechanical planarization (CMP) as the means to brighten the surface and diminish surface irregularities such as bumps, dishes, and rough morphology [22]. Electrochemical planarization methods operate at the limiting current density condition, where the rate of dissolution is limited by the mass transfer rate of a reactant or product. This planarization process etches surface protrusions at an accelerated rate because of their increased proximity to the bulk [22]. Electrochemical polishing or brightening of a surface is also achieved under rate limited conditions, where dissolution is independent of structure [6]. A more site-specific and commonly used form of electrochemical etching is electrochemical micromachining for through-mask passivation or anodic dissolution of a material. This selective etching method is used to fabricate precision inkjet nozzles with specified nozzle angle and undercut as shown in Fig. 13.1 [23]. Mask-free electrochemical micromachining has been demonstrated by the use of ultra short voltage pulses, for appreciable polarization of the double layer only at small electrode separations (microns), resulting in highly localized dissolution of the counter electrode [24].

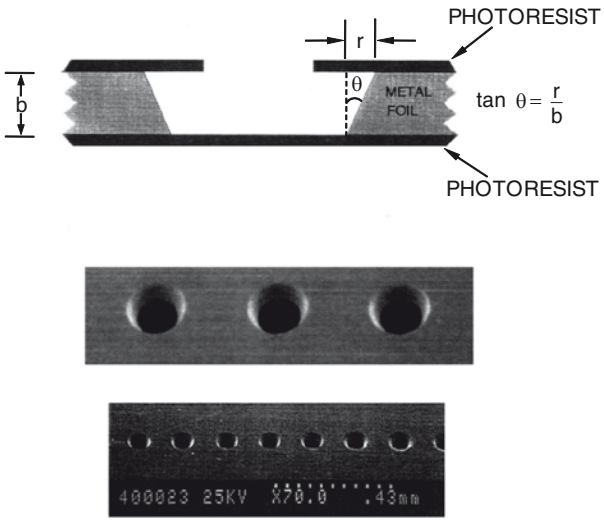

Fig. 13.1 Ink-jet nozzle plate fabricated by through-mask electrochemical micromachining, Schematic of the concept (*top*), and a photograph showing an array of nozzles (*bottom*) [23]

13.3 Top Down Fabrication Approaches

"Top Down" fabrication approaches in the context of MEMS and NEMS technology usually refers to planar, lithographic techniques that are a legacy from Si-based integrated circuit manufacturing [25]. This is where a pre-designed pattern is transferred onto the wafer or other substrate of choice using primarily photolithographic techniques. Optical lithography has made major strides in terms of technological advancement with the recent announcement by IBM's Almaden Research Center of achieving 30 nm features using 193-nm lithography (http://nanotechweb.org/articles/news/5/2/10/1). With regard to electrochemistry-based processing, we have selected the following top–down fabrication topics in MEMS and NEMS.

13.3.1 LIGA

LIGA [26] is a German acronym, short for Lithographie Galvanoformung Abformung. As shown in Fig. 13.2, LIGA is used to create high aspect ratio structures with width to height ratios as high as 1:1000. Recent work at NASA's Jet Propulsion Laboratory (B. Eyre Private Communication 2004) has resulted in the development of axially-symmetric structures with the use of rotating exposure stages. LIGA structures straddle the gap between MEMS and conventionally-machined parts and fall into the so-called "Meso" size range. As shown in Fig. 13.2, LIGA employs collimated synchrotron X-rays that require much more stringent control than optical lithography.

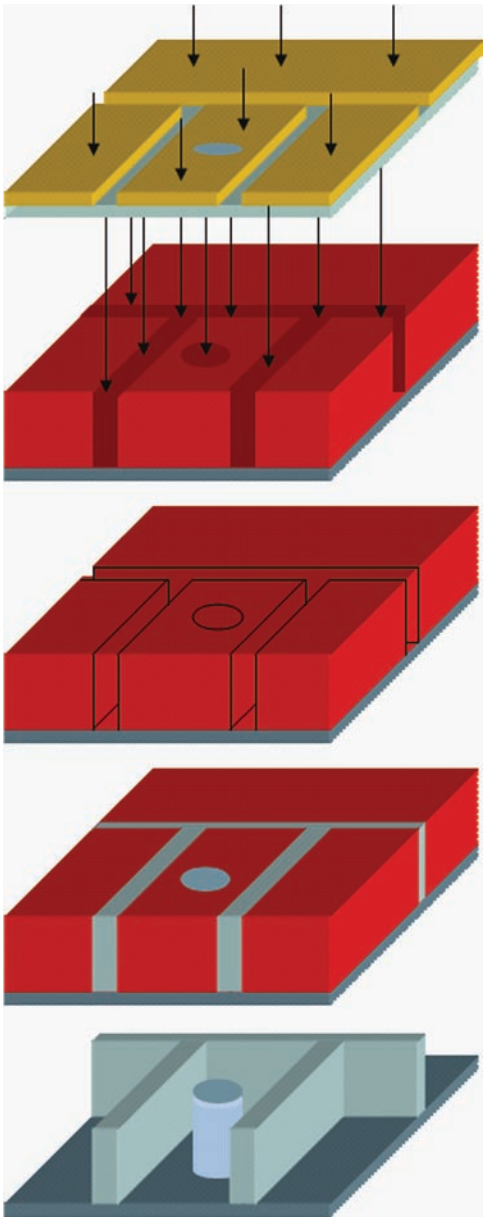

Fig. 13.2 The LIGA process consists of first exposing a thick PMMA resist collimated, synchrotron x-rays. The resist is subsequently developed and a MEMS structure is electroplated within the developed "mold"

An optically generated x-ray mask is itself one of the key features of LIGA, producing the necessary high contrast with a thick (>10 μm) gold absorber on materials membrane consist of low atomic number elements [27]. The absorber mask is patterned using polymethyl methacrylate (PMMA) resists exposed by electron-beam lithography (e-beam) or from an intermediate mask that relies on an e-beam exposure

using a chromium thin film as an adhesion layer. The absorber is then electroplated using a gold plating solution, followed by removal of the PMMA. The critical properties for the electroplated gold absorber are good adhesion and low stress. Intermediate masks are subsequently exposed to x-rays to pattern thicker resists that will ultimately serve as molds for thicker master masks.

LIGA also uses PMMA as a resist to pattern MEMS devices with thicknesses as high as 8 mm. However, in practice, the dimensional tolerances achievable by very thick PMMA resists is degraded significantly by the swelling and thermal expansion of the PMMA caused by absorption of the electrolyte, thereby limiting the maximum height and minimum sizes of LIGA-fabricated features [28, 29]. Although the strain resulting from thermal expansion and absorption of water are minimal for PMMA - 0.2% and 0.4% respectively - dimensions vary significantly for high-aspect ratio LIGA molds. Vertical structures have exhibited lateral offsets as high as 14 μm per mm, with curved features being further distorted [29]. Some of the proposed solutions for reducing linear strain in PMMA are targeted at minimizing thermal expansion effects by using electroplating baths at ambient temperatures or by bonding the resist at elevated temperatures in order to compensate for the thermal expansion and partially for electrolyte absorption. Cross-linked PMMA and alternative resists have also been suggested as alternatives to remedy the absorption problem.

Following exposure, the PMMA is developed much like in conventional photolithography. The conducting back plate for the PMMA is then used as the electrode to create primarily Ni-based electroplated structures within the PMMA mold. These Ni baths have traditionally used sulfur-bearing additives, such as saccharin, as grain refiners that enhance strength and hardness of the plated material. Unfortunately, the mechanical properties of these deposits are rapidly diminished at elevated temperatures, ~600°C, as sulfur groups migrate to grain boundaries causing intergranular fracture.

To alleviate this problem many researchers have turned to Ni–Mn alloys with Mn content of ~1 wt%. While Ni–Mn deposits have been reported with high yield strengths, of which up to 85% can be retained after high temperature annealing, the addition of Mn also increases the residual stress in the deposit. This residual stress problem has been mitigated by pulse plating Ni/Ni–Mn films to create thick structures which have also exhibited increased ductility [30–33]. LIGA fabricated structures have been used for numerous applications including for scroll pump for miniature mass spectrometers (Fig. 13.3) [156].

13.3.2 EFAB™ (Electrochemical Fabrication)

One of the major challenges facing the commercialization of MEMS devices is the cost associated with fabrication of devices with complex geometries requiring tens or potentially hundreds of layers. In this regard, LIGA has fallen short of demonstrating such intricate lamellar fabrication, hindered by the cost associated with numerous layers. Vacuum processes are also unpractical for the fabrication of such multi-layer structures [34]. A new micromachining technology entitled EFAB™

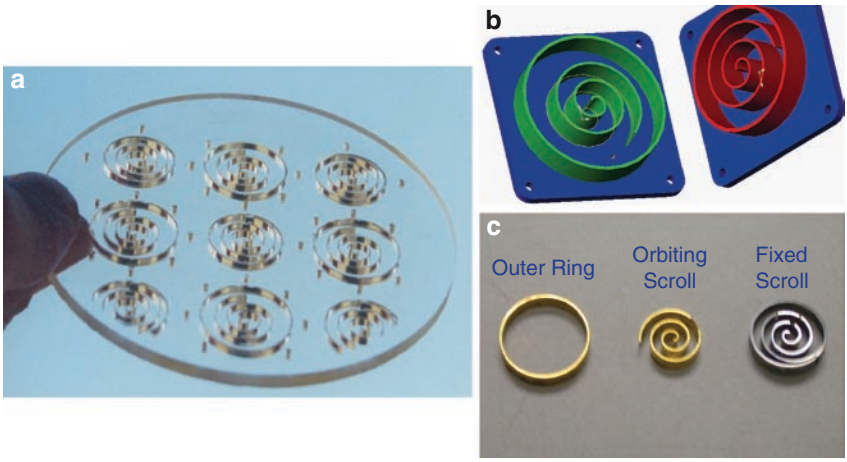

Fig. 13.3 A prototype scroll pump for a miniature GCMS system fabricated using the LIGA process. (**a**) 3 mm PMMA mold, (**b**) schematic of scroll pump, (**c**) electroformed scroll pump

was introduced in 1999, to address the issue of constructing high aspect ratio, three-dimensional, multi-layer microstructures from electroplated metals using a rapid, automated, batch fabrication technique. The core of EFAB™ technology includes an "Instant Mask" process, followed by planarization of each deposited layer. The Instant Mask process is an in-situ masking technique consisting of a pre-patterned insulator that conforms to the surface of the substrate, to allow electroplating of sacrificial material, usually copper, through channels in the mask. This step is followed by blanket-deposition of the structural material, nickel, and planarization, which reduces the need for morphological uniformity, provides precise control over vertical dimensions, and permits the deposition of countless subsequent layers [34, 35]. The device is completed by removal of the sacrificial copper layers through selective etching to release the nickel structure (Fig. 13.4). Although EFAB™ can purportedly create devices from any electrically conductive deposits, material compatibility appears to be an issue as only nickel-based devices have been demonstrated to date.

Since both the sacrificial and structural layers are metallic, EFAB™ can create overhangs, extruded shapes, and disconnected features, but lacks the ability to integrate dielectrics [34]. This is detrimental for the production of fluidic and bio-MEMS which benefit from the low-cost, biocompatible interfaces of plastic microstructures [36]. EFAB™ can currently achieve lateral minimum feature sizes of 20 microns - significantly larger than minimum feature sizes possible using other microfabrication techniques - but has demonstrated vertical feature sizes as low as 5 microns, an advantage of its layer by layer synthesis. However, the key advantage of EFAB™ is that it does not require a cleanroom with stringent environmental and particulate control requirements. Its fabrication process strengths include mild

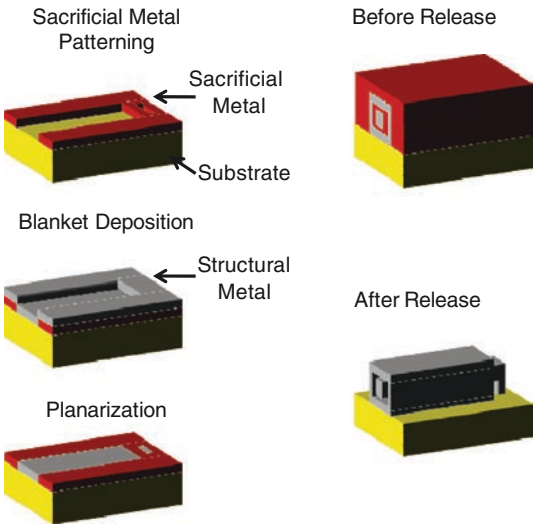

Fig. 13.4 The EFAB process flow used to fabricate a hybrid coupler (Permission from Microfabrica Inc.)

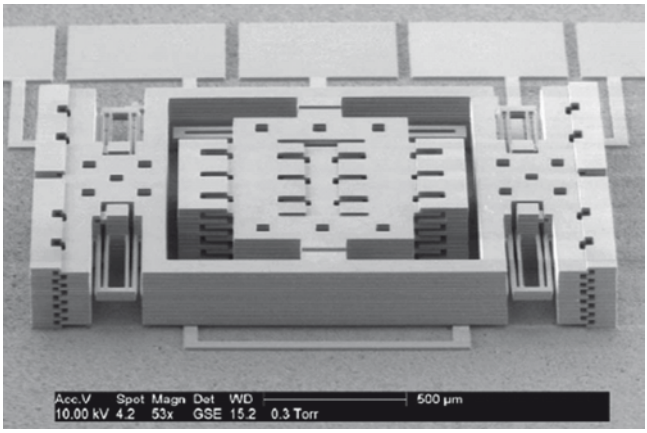

Fig. 13.5 SEM picture of the fabricated nickel gyroscope. The gyroscope occupies an area of 2.1×1.3 mm^2 [37]

electroplating conditions, 60°C ambient, and in-situ masking, all of which are amenable with the low temperature requirements for IC processing. Despite its relative "youth" as a fabrication technique, EFAB™ has already demonstrated its versatility in creating a number of otherwise challenging structures such as rectangular coaxial conductors, helical inductors, accelerometers, toroidal inductors, variable capacitors, and a microgyroscope (Fig. 13.5), [37, 38].

13.3.3 Electron Beam Lithography of NEMS Structures

Electron Beam Lithography (EBL) has gained considerable recognition as a very capable "top–down" nanofabrication technique when coupled with electrochemical processes, allowing precise control of nanostructures that are not possible using complex self-assembly techniques. In-situ fabrication techniques are possible by combining lift-off processes with EBL in order to prepare the substrate for directed nanowire growth. In fact, using directed growth techniques, electrochemically deposited nanowires can be made to laterally bridge the gap between two micro-electrodes by confining the nanowire to grow within an EBL fabricated channel in polymethyl methacrylate (PMMA) [39] (Fig. 13.6). These nanowires can be grown laterally, simultaneously from each micro-electrode, either potentiostatically or galvanostatically. Completion of the bridge is indicated by a jump in the corresponding current or potential when contact is made between the two ends of the nanowire. Synthesized nanowires are individually addressable and can span lengths of micrometers with diameters limited only by EBL techniques [40]. Various sensing materials such as palladium, polyanaline, and polypyrrole have been investigated for chemical and biological sensor applications demonstrating the potential for high density arrays of nanowires [40–42]. Precise four-point conductivity measurements of nanowires have also been conducted using built in micro electrodes [43].

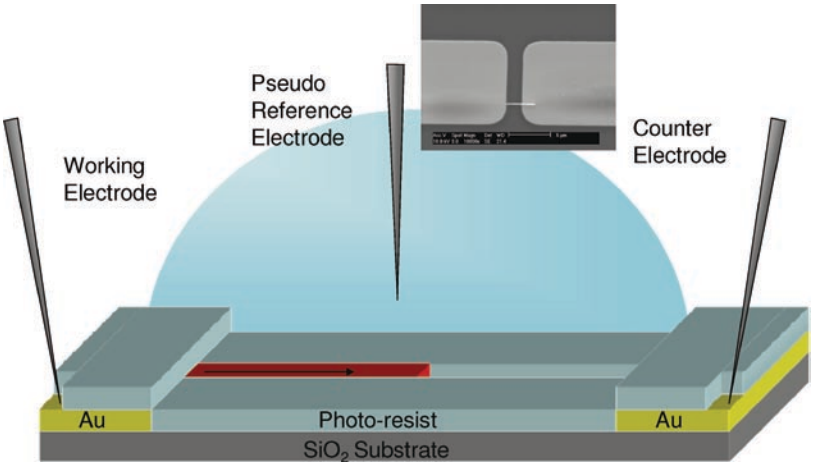

Fig. 13.6 In-situ nanowire synthesis: The working electrode and counter electrode are contacted by probe tips. A probe tip is also used as a pseudo reference electrode, submerged in the solution containing the analyte. The nanowire (*red*) is growing in the direction of the arrow, from the working electrode to the counter electrode, confined to a predetermined path by the photoresist. The inset shows an SEM micrograph of a polypyrrole nanowire fabricated by in-situ synthesis

13.4 Bottom Up Fabrication Approaches

The "bottom up" approach to NEMS and MEMS is still very much in developmental stages with few commercially available devices. With current MEMS/NEMS products relying significantly on top–down processes, the bottom up approach is being integrated into certain application niches where they provide cost reduction and performance enhancement over conventional techniques. While current research has actively pursued the investigation of nanowires and carbon nanotubes (CNTs), spatial manipulation and addressability remain crucial hurdles that must be overcome in order to realize their full potential. The construction of novel MEMS/NEMS devices from nanostructures remains the subject of many research activities, aimed at arranging these nanowires in some ordered fashion, with either an applied energy field or through surface functionalization, and thereby enabling the use of nanowires and CNTs for sensing functions. In this section we present current electrochemical techniques for bottom up nanostructure synthesis and methodologies for assembling these nanowire structures.

13.4.1 Template-Based Nanostructure Synthesis

The bottom up approach to MEMS and NEMS has been significantly impacted by electrochemistry-based template synthesis techniques. A popular approach is the use of nanoporous templates as working electrodes by sputtering or evaporating a thin conductive layer on one side of the template [44–46]. The template acts as a scaffold to confine the electrodeposited material within the nanopores thereby producing nanostructures ranging from nanodots to high aspect ratio nanowires. Following deposition, the seed layer is removed and the template is etched to release the nanowires in suspension (Fig. 13.7). The power of template synthesis approach lies in both its simplicity and highly parallel manufacturability, with template pore densities in the range of 10^{9}–$10^{11}\,cm^{-1}$ and also in providing a platform for array applications or more complex structures, ultimately through template removal and assembly [47].

A diverse spectrum of materials is amenable to the production of electrodeposited nanowires. This includes magnetic materials, semiconductors, metals, alloys, and conducting polymers [44–46]. Complex, multicomponent nanostructures such as superlattice nanowires can also be deposited from a multielectrolyte solution by modulating the voltage or current. The requirement for these electrolytes is that they should have a substantial difference in their deposition potentials starting with the nobler elements at lower concentrations. Segmented nanowires can also be produced by switching the electrolyte baths during the deposition process [47]. The switched-bath method has been used to successfully produce metal/semiconductor, conducting polymer/semiconductor, and conducting polymer/metal heterostructures [48–50]. Surface modified templates have even been used to investigate core/

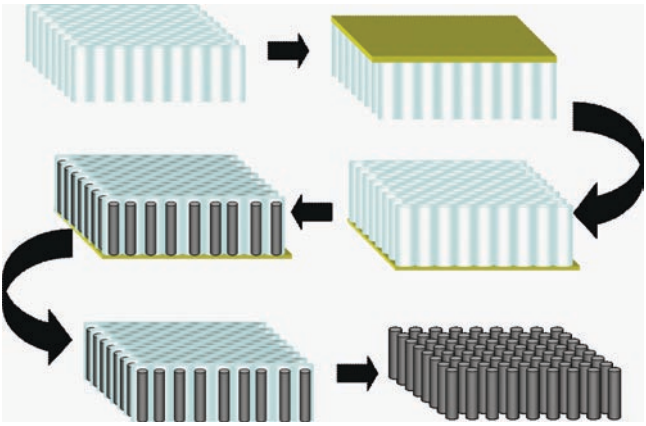

Fig. 13.7 Template Synthesis: A conductive seed layer is sputtered on the backside of the template. The nanowires are electrodeposited in the template. The seed layer is removed by physical or chemical means. The template is dissolved to yield a colloid of nanowires in solution

shell structures as well as molecular imprinting on the surface of conducting polymer nanowires [51, 52].

All these nanostructures, though simple by design, are crucial for performing complex functions. A polypyrrole nanowire, which is essentially an n-type semiconductor, could be a resistor in a single component form. However, when coupled with a Cd segment the nanowire acts as a p-n junction, and can be used as a diode-rectifier. For good ohmic contacts, Au segments can be electrochemically added to both ends of the same wire. Such a device was recently demonstrated and characterized by Mirkin's group, as shown in Fig. 13.8a and b [53]. Similarly Ni/Cu superlattice nanowires can also be produced for one-dimensional Giant Magneto Resistive (GMR) properties by adjusting layer thickness and composition. The core shell design has been used to create coaxial nanowires, consisting of an Au/CdS/Au nanowire sheathed within SiO_2, and implemented in a field effect transistor (Fig. 13.8c and d) [54]. In addition to mimicking traditional electronic components with nanowires, electrodeposited materials can also be incorporated for spatial manipulation via applied energy fields or surface functionalization. However, as these nanostructures increase in complexity, they also become more susceptible to mechanical breakage and poor interfacial adhesion. These mechanical limitations often result in these structures being demonstrated first in the submicron range, precluding quantum confinement effects. Similarly, many materials fabricated by template synthesis technique are characterized in array form, whereby the template provides mechanical support to the nanowires of interest. Although many of the materials and structures studied are precursors to further miniaturized, complex systems, investigations of these one-dimensional entities have elucidated new fundamental phenomena and stimulated creative, nanowire-based device design and fabrication. Therefore, template synthesis and post synthesis manipulation are important techniques which merit further discussion in the section below.

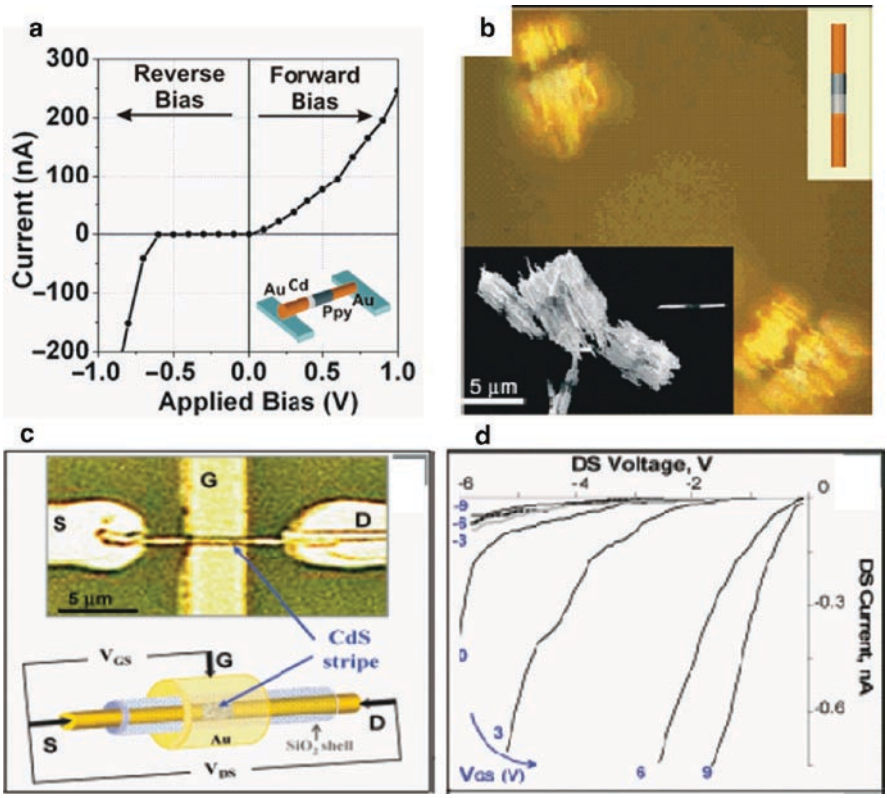

Fig. 13.8 (**a**) *I-V* characteristics for a single Au–Ppy–Cd–Au rod at room temperature. (**b**) Optical microscope image of Au–Ppy–Cd–Au rods. The lower left inset shows the corresponding field emission scanning electron microscopy (FESEM) image [53]. (**c**) Optical micrograph and schematic drawing of the test structure and Au/CdS/Au@(SiO2)10 nanowire aligned for measurement of electrical properties. Letters S, D, and G indicate source, drain, and gate electrodes, respectively. (**d**) Typical *I*DS-*V*DS characteristics of in-wire TFTs for different values of gate voltage (*V*GS), 11 devices measured. Reprinted with permission from ref. [54]. Copyright (2004) American Chemical Society

13.4.1.1 Anodic Alumina Templates

Anodic alumina has been the most rigorously investigated material for template synthesis, with early work dating as far back as the 1950's [55]. Characterized by highly ordered, vertically parallel pores, it is one of the most densely packed porous structure at approximately 10^{11} pores/cm^2. Anodic alumina templates can be fabricated to produce pore sizes ranging from a few nanometer to several hundred nm in diameter [56]. The pores are formed by anodizing the surface of high purity (99.999%), and often preannealed aluminum. The pore nucleation is initiated locally by the electric field distribution, with pore growth being determined by the chemical equilibrium at the electrolyte/oxide interface and the oxide/metal inter-

face [55]. The alumina pore sizes and interstitial spacings are controlled by the electrolyte type, concentration, voltage, and temperature. Under appropriate conditions, a "self assembly" process takes place, with individual nanopores growing to form a close-packed assembly of vertical honeycomb structures. Individual pores with this assembly are separated from each other and from the underlying aluminum substrate by an insulating barrier layer of aluminum oxide [57]. After anodization is complete the barrier layer can be penetrated either by an ion milling step or by a two step etching process [58]. The etching method involves removal of the residual, elemental Al with either $HgCl_2$ or $CuCl_2$ solution followed by the barrier layer removal or pore widening step using phosphoric acid [59, 60].

The order of the pores over large areas greater than several microns is limited by the heterogeneity in the pore initiation defects. A two-step anodization technique has been employed in order to mitigate these defects [60]. The Al substrate surface is first electropolished using a strong acid mixture such as perchloric acid and ethanol followed by long period anodization. A first, long duration anodization step is conducted in order to produce an ordered structure at the substrate interface via pore coalescence. The anodized layer is subsequently removed to yield a surface of patterned concave formations. These concave indentations serve as starting points to initiate a highly ordered hexagonal configuration of pores over large areas of the template surface (Fig. 13.9) [60]. Masuda and coworkers have also developed a similar method relying on lithographically produced molds to pre-texture the surface with an array of dimples. These indentations serve as pore initiation sites in a similar manner to the concave indentations produced in the two step anodization process [61]. The versatility of these anodized aluminum templates extends to three-dimensional structures, including cylinders and multifaceted objects [62]. Alumina templates can also be easily integrated into existing CMOS technologies, by utilizing a wet etching technique for creating complex shapes with vertical side walls [63] Lateral anodic oxidation of Al thin films has also been established on SiO_2 substrates. [64]. These pores were observed to be ordered and parallel to the substrate surface with diameters as low as 3 nm, thus paving the way for more complex configurations.

13.4.1.2 Track-Etched Templates

Membranes suitable for "track etching," such as mica and polycarbonate (Fig. 13.10a), use heavy charged particles from a nuclear radiation source to generate tracks of radiation damage within the material. These high-energy particle tracks within these membranes are subsequently chemically etched to produce uniform pores with diameters determined by etching time. Side-wall tapering for the pores is minimal because of the high etching rate selectivity along the tracks in comparison to the lateral etch rate [65]. Mica is a unique membrane material in that its pores are diamond shaped with the same size and orientation for all pores. This feature has been shown to be consistent across a wide range of mica samples, with the aspect ratio being governed primarily by the crystal structure of material [65, 66].

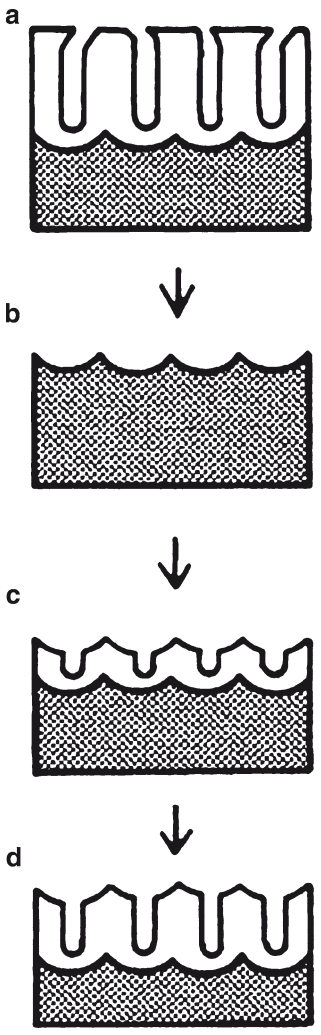

Fig. 13.9 Schematic diagram for two step anodization: (**a**) porous alumina after first anodizing, (**b**) removal of porous alumina layer, (**c**) initiation of hole formation in second anodizing, (**d**) porous alumina after second anodizing. Reprinted with permission from ref. [60]

The primary drawback to the use of these mica templates are the very low pore densities, 10^9 pores/cm, and randomness in the lateral ordering of the pores [47]. Polycarbonate templates, which also exhibit track-etching behavior, have the further complication of being susceptible to swelling during electrodeposition, consequently giving rise to large variances in the pore diameter, resulting ultimately in cigar-shaped or conical nanowires [67]. Track-etched pores generated on commercially available polycarbonate templates have been shown to have random orientations resulting in poor properties for nanowire arrays fabricated within these templates. However, it is possible to control pore quality and inter-pore separation distances

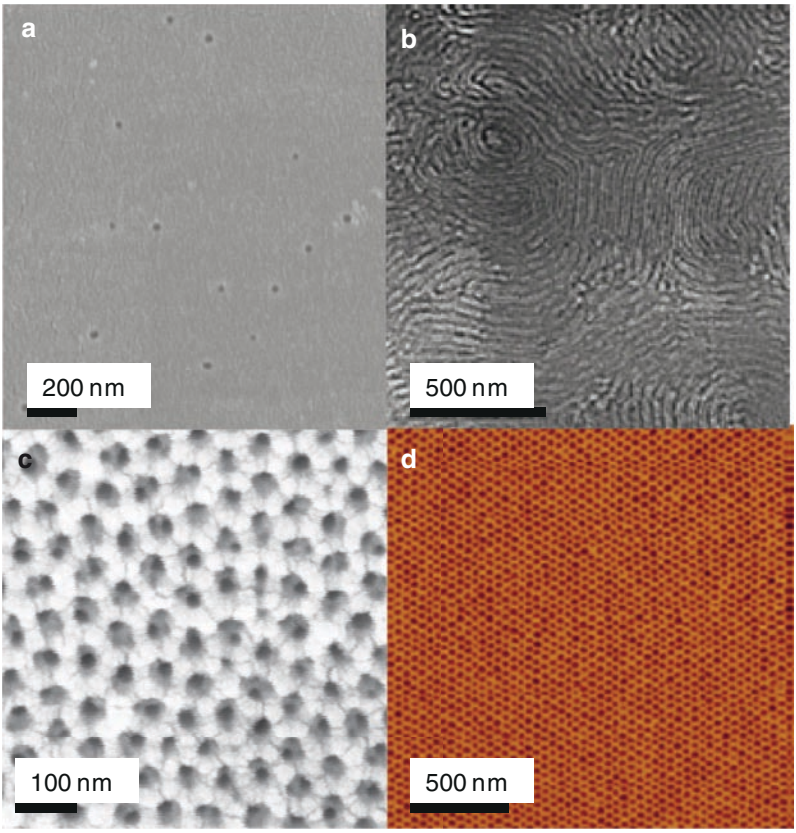

Fig. 13.10 Various materials used in template synthesis; (**a**) Polycarbonate (**b**) Silica [74] (**c**) Alumina (**d**) Diblock Copolymers. Figure 13.10b reprinted with permission from ref. [74]. Figure 13.10d reprinted with permission from ref. [155]

by optimizing the distance between the template and the particle source [65]. These templates have been fabricated with pores as small as 8 nm and commercially available templates with 15 nm pores [68].

13.4.1.3 Silica Templates

Considerable amount of research has gone into the development and characterization of surfactant templated silica, in order to produce various mesophases and nanowire geometries with well-controlled pore diameters within the quantum confinement regime (i.e. 2–20 nm). Lu and coworkers have characterized one of the more promising methods, a sol-gel dip-coating method for rapid (tens of seconds) template generation. The fabrication process involves evaporation-induced self assembly of liquid crystal domains dominated by inward growth from the solid-liquid

and liquid-vapor interfaces [69–71]. The resulting mesophase is manipulated by controlling the surfactant type and concentration whereby a progression of structures from hexagonal through cubic to lamellar is observed with surfactant enrichment. These mesophases are capable of yielding either one-dimensional pores or three-dimensional interconnected pore structures (Fig. 13.10b). The surfactant/silicate thin films are subjected to calcination at 400°C to remove the surfactants producing the nanoporous silica [72]. By incorporating a conductive substrate for the sol-gel dip-coating process, nanowire arrays or a nanomesh can be electrodeposited within the one-dimensional and three-dimensional pore structures [73, 74]. Lu's group has also extended this fabrication method to hexagonal, cubic, and vesicalar structured spherical nanoparticles by aerosol-assisted self assembly [70].

13.4.1.4 Diblock Copolymer Templates

Immiscible polymers have attracted significant interest as the materials for self assembled templates for nanowire production (Fig. 13.10d). By covalently bonding together polymers with different interfacial energies, phase separations occur at the nanoscale level with highly oriented and periodic domains [75, 76]. Thin films of lamellar, cylindrical, and spherical microdomains have all been formed with tunable dimensions controlled by the polymer chain lengths or molecular weights [75, 77]. Common copolymers include polystyrene (PS) and polymethylmethacrylate (PMMA) denoted PS-*b*-PMMA, and polystyrene and polyethyleneoxide (PEO) denoted PS-*b*-PEO. Current PS-*b*-PMMA copolymer thin films with cylindrical domains are synthesized by spin coating followed by annealing for 12–24 h under an electric field of 30–40 V/μm at a temperature above the glass transition temperature of both polymers. The applied voltage induces alignment of the cylindrical domains with the orientation of the electric field [78]. Xu and co-workers have shown that small concentrations of Li ions contribute to the electric field alignment of the PMMA cylinders [79]. The ensuing matrix is subsequently exposed to ultraviolet light, which degrades the PMMA while simultaneously cross-linking the PS [80]. These self-assembled polymer templates are a promising platform for the creation of future MEMS and NEMS structures, by facilitating both lateral and vertical growth of nanowires with diameters down to 5 nm [81] (Table 13.1).

13.4.1.5 Alternative Nanostructure Synthesis

Biotemplates have been fabricated from two-dimensional crystalline surface proteins for the subsequent electrochemical deposition of nanowire structures [82]. These surface layer proteins encapsulate certain bacterial cells, controlling extracellular transport. They form especially robust thin films over cells, and are resistant to conditions that normally denature proteins, such as low pH and heat, thus making them ideal as template materials for electrodeposition. Schwartz and coworkers investigated a hexagonally packed intermediate surface layer protein from

Table 13.1 Comparison of different templates parameters for synthesis of nanowires and references for various materials fabricated with each template

	Alumina	Polycarbonate	Mica	Silica	Copolymers	Biotemplate
Pore diameter (nm)	4–500	15–1,000	8–1,000	2–40	5–50	2–3
Pore density	10^{11}	10^{9}	10^{9}	10^{11}	10^{11}	10^{11}
Pore packing	Hexagonal	Random	Random	Cubic, Hexagonal	Hexagonal	Hexagonal
Pore tilting	No	Yes	Yes	No	No	No
Thickness (μm)	10–100	6–20	10–70	2.5	1–5	0.005–0.006
Macroscopic range	Centimeters	Centimeters	Centimeters	Microns	Microns	Microns
IC Compatability	Yes	No	No	Yes	Yes	Yes
Lateral Growth	Yes	No	No	No	Yes	No
Swelling	No	Yes	No	No	No	No
Geometry	Cylindrical	Cylindrical	Diamond cross section	Cylindrical, Mesh	Cylindrical, spherical	Cylindrical, ring
Solubility	Strong Acids or Bases	Chloroform, Dichloromethane	Strong bases, HF	HF	Organic Solvents, Toluene	
Metals	Martin 1995 [45]	Staufer 1997 [67]	Possin 1969 [157]	Lu 2003 [74]	Russell 2000 [80]	Schwartz 2005 [82]
Magnetic materials	Martin 1995 [45]	Staufer 1997 [67]	Chien et al. 1999 [66]	Luo et al. 2005 [158]	Russell 2000 [80]	Schwartz 2005 [82]
Semiconductors	Klein et al. 1993 [159]	Sima et al. 2004 [160]	Mukherjee and Chakravorty 2004 [161]	Wang et al. 2006 [162]		Schwartz 2005 [82]
Conducting polymer	Martin 1995 [45]	Staufer 1997 [67]				
Metal oxides	Li et al. 2000 [163]					Schwartz 2005 [82]

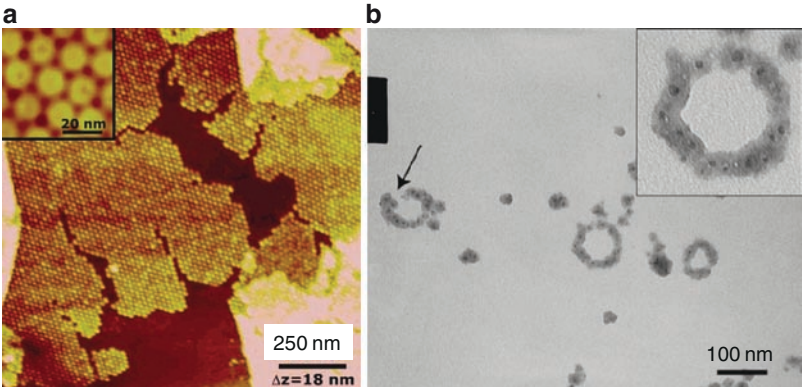

Fig. 13.11 (**a**) Tapping mode AFM image of HPI layer proteins on a polished steel disk reveals typical coverage when proteins are contacted for several minutes before washing. Inset: higher resolution image on freshly cleaved mica revealed patterned arrangement of channels. (**b**) TEM images of Cu2-TraIi1753:CN225 nanoparticles self organized on circular X174 RFII DNA. Nanoparticle loops are never observed in the absence of circular DNA additions. The arrow identifies an incompletely decorated loop. Figure 13.11a reprinted with permission from ref. [82]. Copyright (2005) American Chemical Society. Figure 13.11b reprinted with permission from ref. [83]. Copyright (2005) American Chemical Society

Deinococcu radiodurans, with 2–3 nm pores and widths of 5–6 nm (Fig. 13.11). The surface layer proteins were bound to the cells by hydrophobic interactions and were extracted using a detergent, sodium dodecyl sulfate (SDS). The resulting templates have been randomly dispersed on conductive substrates for through-mask deposition of Cu_2O, Ni, Pt, Pd, and Co [82].

Schwartz and co-workers have also investigated hybrid inorganic-protein moieties for the assembly of unique three-dimensional nanostructures [83–85]. The DNA binding protein Tral was engineered with a polypeptide binding sequence for Cu_2O, and optimized using cell adhesion assays on a quartz crystal microbalance. The binding sequence was also designed with an absence of cysteine groups to eliminate the possibility of thiol-mediated metal center binding, resulting in loop formation by oxidation of the flanking cysteine thiols. The binding affinity (K_d) of the engineered Tral for Cu_2O was determined to be 1.2×10^{-8} M. The DNA binding sequence was also preserved, as demonstrated by the self assembly of protein bound Cu_2O particles binding to cyclic DNA [83]. This technique shows promise for the assembly of multi-dimensional nanostructures based on DNA-positive templating.

Selective electrochemical deposition (SED) at the edge planes of highly oriented pyrolytic graphite (HOPG), or electrochemical step edge decoration (ESED), has been utilized to fabricate nanowires from metals, metal oxides, semiconductors, and bimetallics by Penner and co-workers [86–90]. Although this method does not fall under the class of template synthesis, still, the step edges of HOPG could be considered as a positive template. Nucleation is preferentially initiated on the step edges, where the sp^2 bonds of the basal plane are terminated and a line of higher

surface energy/chemical reactivity occurs [91, 92]. The nanowires are formed by the coalescence of adjacent nucleation sites on the step edge, with the minimum nanowire diameter coinciding with the diameter of the nuclei at the point of coalescence [93]. These step-edge nanowires have hemi-cylindrical cross sections and can reach lengths of several millimeters [94]. Metal oxide nanowires can be directly deposited on the step edge by employing small overpotentials. The selectivity of preferential nucleation at step-edge sites is sensitive to the overpotential value, with greater overpotentials leading to significant deposition on the terraces as well. A "tri-potential" process is used for the deposition of noble metals such as Ni, Cu, Ag, and Au. The step edge defects are first activated with a positive potential for several seconds; nucleation at step-edge sites is then initiated with a high overpotential for several milliseconds, with subsequent reduction in the overpotential for the coalescence of adjacent nuclei to grow the nanowires (Fig. 13.12) [88]. Arrays of metal nanowires can be extracted from the HOPG substrate using a polystyrene or cyanocrylate adhesive. Metal oxide nanowires however, must first be reduced to metal (annealing under hydrogen) to have the necessary mechanical integrity required to survive the transfer from the HOPG substrate [95].

Carbon nanotubes are responsible for spawning the age of nanotechnology, and creating a paradigm shift in our views on materials and their applications. In the field of MEMS and NEMS, CNTs have found applications as electromechanical switches or as pliable nano-actuators, among others. The high elastic modulus of

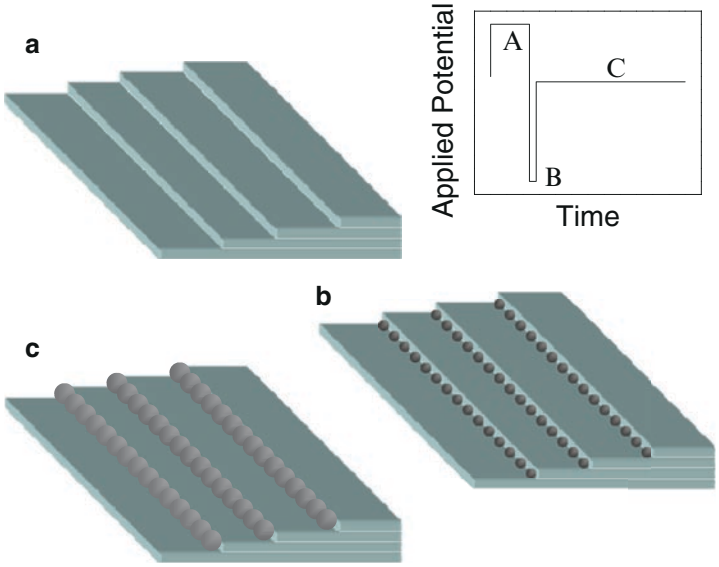

Fig. 13.12 ESED of noble metals is a tri-potential sequence (inset). (**a**) First the HOPG step edges are oxidized to form carboxyl groups, disrupting edge sp^2 bond, (**b**) deposition is initiated with nucleation sites at the edge plane from a low potential pulse, (**c**) followed by a low overpotential step for subsequent growth of the nucleation sites to the coalescing point

CNT has already been exploited in NEMS as the basis for a rotary element for a magnetically actuated nano-plate [96] and additional NEMS devices relying on both the novel mechanical and electrical properties of CNTs will continue to be developed in the years to come. Composite materials containing CNTs, especially inorganic material/CNT blends, have been demonstrated to have enhanced mechanical and tribological properties, unattainable with current metallurgical techniques [97]. These electroless and electrodeposited composites will provide a new class of materials available for MEMS and NEMS devices.

In addition to codeposition, metal/CNT composites can also be formed by electrochemically coating CNTs. Recent efforts to characterize various electrochemical coatings on CNTs have discovered unique charge transport behaviors in hybrid inorganic/CNT structures, which can be exploited for sensing applications [98]. However, to date, only a handful of materials have been electrochemically coated on CNTs (e.g. Ni, [97] Au, Ag, and Pt [99]). These studies have elucidated the mechanism of nucleation for electrodeposited materials on networks of single wall carbon nanotubes (SWNT) to create nanoparticle and nanowire coatings [99]. Both the type of electrodeposited materials and the potential gradient along SWNT networks were shown to influence the number of nucleation sites created and the subsequent coalescence and growth of the deposit. In all cases, electrodeposits on CNT networks were shown to form nanowire coatings with higher density nucleation and hence smaller nuclei closer to the working electrode, moving to larger particles, on the order of microns, that became sparser with increased distance from the electrode [99]. In addition, the ends of the nanotubes as well as defects within the nanotubes have been shown to be areas of high electrochemical and chemical reactivity, in a similar fashion as the edge planes in ESED, with enhanced electrochemical deposition occurring at these sites [91, 92]. These mechanisms of nucleation and growth are the subject of in-depth studies of CNT surface chemistry affecting electrodeposition. Thus, electrochemistry has played a key role as an important fabrication technique for CNT-based coatings, composites, and also as a means for providing conductive contacts for electrically addressing CNTs.

13.4.2 Template-Free Nanowires

Although a large majority of electrochemically fabricated nanowires use templates, there has also been considerable work reported on the generation of freestanding nanowire networks by either chemical or electrochemical means [100–103]. While chemical methods rely on polymerization at an aqueous/organic interface [101] or nonselective coverage of a substrate, electrochemical deposition involves site-directed growth between electrodes, and has been used successfully for creating conducting polymer nanowire electrode junctions (CPNEJs) [104]. A continuous, three-step galvanostatic method is utilized to fabricate the electrodeposited nanowire junctions. The first step requires the use of a high current density - 0.08 mA/cm^2 - for 30 min for the deposition of polyaniline, in order to initiate nucleation of

polymer nanoparticles on the working electrode. During the second and third steps, nanowire growth propagates at lower current densities, 0.04 mA/cm^2 for 3 h and 0.02 mA/cm^2 for 3 h, respectively. The resulting nano-mesh can span a 2 μm gap with ligament diameters in the range of 40–80 nm, which correspond to the diameters of the nuclei produced during the first step. Polyaniline, polypyrrole, and polyethylenedioxythiphene (PEDOT) have all been used to make CPNEJs with high reproducibility and scalability for applications involving the detection of gaseous analytes [104].

13.4.3 Novel Assembly Techniques

13.4.3.1 Langmuir Blodgett Techniques

To date, a proven and robust technique for assembling large arrays of nanowires is the Langmuir-Blodgett (LB) technique. These nanowire-based thin films can be fabricated with controlled pitches and are also amenable to layering for the creation of more complex structures [105–108]. The LB process begins by surface functionalization of the nanowires with long alkyl chains. Once these functionalized nanowires are introduced into the sub-phase, or aqueous component, they selectively partition to the water-air interface because of their hydrophobically rendered surfaces. At low pressure, the nanowires are aligned isotropically on the surface as side-by-side aggregates called "nano-rafts" formed as a result of directional capillary forces and van der Waals forces [109]. With increased surface pressure created by compressing the trough container, the nanowires begin to align parallel to the trough wall, creating a two-dimensional nematic phase. Further compression pushes the monolayer into a smectic arrangement with uniaxial alignment and high precision spacing (Fig. 13.13). Above a certain critical pressure, the maximum areal density of the monolayer is surpassed, transitioning the nanowire film into multilayers or a three-dimensional nematic phase containing singularities [109]. The close-packed LB monolayers in the smectic regime are preferred for device

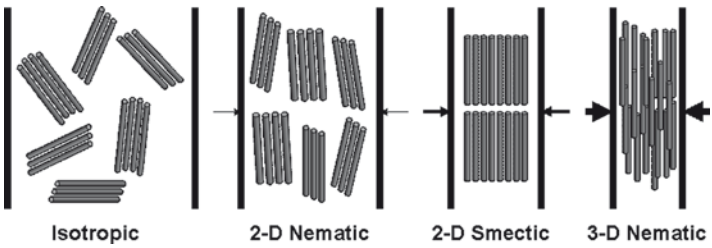

Fig. 13.13 Schematic of Langmuir–Blodgett monolayers. As the trough wall are pushed in, indicated by the arrows, the surface pressure is increased and the nanowires transition through the sequence of phases; isotropic, 2-D nematic, 2-D smectic, 3-D nematic

fabrication, as they have well-defined, uniform pitches with axial length scales of up to a centimeter [105–108].

13.4.3.2 Magnetic Alignment

The high aspect ratios of magnetic nanowires impose a shape anisotropy that only allows magnetization along the axial direction with only two possible orientations for the polarity [65]. The resulting magnetically polarized nanowire can be manipulated with external magnetic fields, ferromagnetic substrates, and neighboring magnetic nanowires. Magnetic interactions were first investigated as an approach to manipulate nanowires by Searson and co-workers [110]. Using ferromagnetic nanowires they demonstrated real time end-to-end alignment in solution, with the velocity of alignment being directly proportional to attractive forces between nanowires and inversely proportional to viscous drag in solution [110]. Searson later demonstrated the entrapment of a multi-segmented Pt/Ni/Pt nanowire between two Ni pads with a 135 Oe remnant magnetization from previous exposure to a 10G magnetic field. Although the remnant magnetization was sufficient to entrap nanowires, the success rate was greatly enhanced with an applied magnetic field, as the applied field facilitated alignment of the nanowires between the electrodes and reduced aggregation [111]. Crone's group successfully demonstrated the entrapment of an inversed nanowire structure to Searson's magnetically entrapped nanowire, consisting of a bronze midsection with ferromagnetic caps and aligned between Ni stripes [112]. Subsequently, Myung and coworkers have investigated the effect of ferromagnetic pad geometry and magnetic field strength for controlling the directionality of nanowire assembly (Fig. 13.14). Nanowire chaining and agglomeration was minimized by dilution (Fig. 13.15). A solder thin film was electrodeposited on Ni electrodes for the purpose of making robust electrical contacts to the Ni/Bi/Ni nanowires [113]. Myung and coworkers were the first to demonstrate magnetic assembly of true nanowires, with diameters of 30 nm, on gold and nickel electrodes, using an annealing step to achieve ohmic contact for magnetic and electrical measurements [114]. Magnetic alignment has also been demonstrated for structurally modified CNTs, where the modified CNT has a magnetic catalyst nanoparticle on one terminal end and a thermally evaporated Ni cap on the opposite end [115].

13.4.3.3 Electric Field Alignment

Electric field assisted assembly is applicable to a wide range of materials including semiconductors, metals, and CNT's, as opposed to being restricted to only ferromagnetic materials for magnetic alignment [116–118]. Electric field assisted assembly utilizes an alternating current to polarize nanostructures for assembly purposes or for other dynamic functions. Mallouk and coworkers were the first to demonstrate electrical alignment of Au nanowires, citing the voltage and the frequency as the main parameters controlling the alignment time.

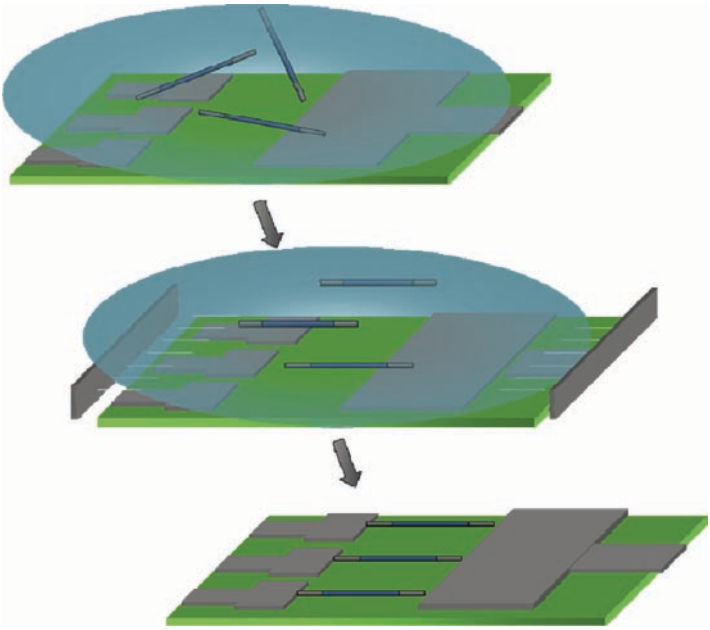

Fig. 13.14 Schematic for magnetic alignment. (**a**) A colloid initially contains randomly oriented nanowires. (**b**) The nanowires align parallel to an applied magnetic field (**c**) and position between ferromagnetic substrates

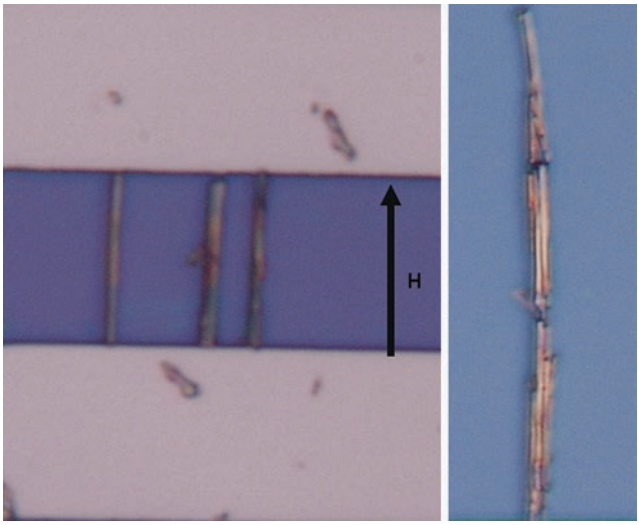

Fig. 13.15 Optical images of (**a**) Ni/Au/Ni nanowires aligned parallel to an applied magnetic field, inplane and adjacent to the nickel electrodes. (**b**) Ni/Au/Ni nanowires form chains in the absence of ferromagnetic electrodes to direct placement. The arrow indicates the direction of the applied magnetic field

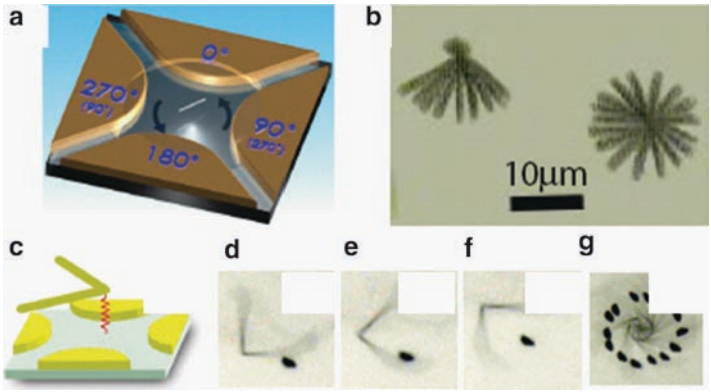

Fig. 13.16 (**a**) Schematic of a nanowire suspended in DI water set to rotation by quadruple electrodes, at which four phase-shifted ac voltages are simultaneously applied but with a sequential phase shift of 90°. (**b**) Overlapped images at 1/30 s interval of free (*right*) and on end fixed (*left*) rotating Au nanowire at 2.5 V, 80 kHz. (**c**) Schematic of a bent nanowire attached to the surface. Snap shots (**d**)–(**f**) of rotating bent nanowires taken every 1/30 sec and (**e**) overlapped images taken within 1.8 s under 10 V at 20 kHz illustrating a bent nanowire as a micromotor driving a dust particle. Reprinted with permission from ref. [121]. Copyright (2005) by the American Physical Society

The movement of nanowires within an electric field is dependent on its polarization within the surrounding dielectric medium. The electric field induces a dielectrophoretic force on the nanowire in the direction of the electric field [117]. Studies on dielectrophoretically controlled nickel silicide nanowires also revealed mechanisms for "chaining" and branching interactions among nanowires. The induced dipoles orient the nanowires parallel to the electric field while simultaneously creating localized coulombic attractive forces between adjacent nanowires resulting in their forming chains. Pre-aligned nanowires positioned on top of electrodes experience an enhanced electric field, consequently attracting other nanowires in solution along the radial direction, thereby stimulating branching structures [119]. Controlled rotation of nanowires has also been carried out by Chien's and Bhiladvala's groups using a quadruple electrode setup with simultaneously applied voltages with sequential phase shifts of 90°, thereby creating a "nanomotor". These devices have been demonstrated for free standing nanowires as well as for fixed nanowires (Fig. 13.16a and b) [120, 121]. A bent Au nanowire motor tethered to a thiolated substrate is also shown in Fig. 13.16.

13.5 Applications

From a practical standpoint, electrochemical fabrication is currently used primarily in LIGA or EFAB, the predominant electrochemical techniques for fabricating MEMS devices. Electroplating can be used to mimic certain forms of silicon

processing or can actually substitute for these processes. The cost and associated trade-offs in using electrochemical processing, are a strong function of the exact process, desired device performance, material properties, and process limitations. Electrochemistry is also the subject of active research aiming at developing greater understanding of electroplating technology and the relationships between material properties and structure [6]. Template synthesis is the dominant electrochemical fabrication method currently being used to fabricate NEMS devices. Here we present some of the more innovative devices in MEMS and NEMS with particular focus on nanowire-based systems.

13.5.1 MEMS Example: Force-Detected Nuclear Magnetic Resonance Spectrometer

NMR spectroscopy can be conducted using two, very different approaches: the conventional, Faraday-law detection technique and the force-detection technique described below. In both cases, the NMR signal is derived from RF excitation of the sample's nuclear magnetic moment. In the conventional technique, detection occurs by virtue of the induced current in a detector coil generated by the cyclic inversion of the nuclear magnetic moment. FDNMR on the other hand relies on measuring the dipole-dipole force interaction between the sample's nuclear spin magnetic moment and a small detector magnet (of equivalent size to the sample) located in the vicinity of the sample (Fig. 13.17). The FDNMR spectrometer is constructed using MEMS fabrication techniques [122]. The detector magnet is mounted on a microfabricated Si beam making up a mechanical resonator. The detector magnet sits within an annular magnet (Fig. 13.18), thus providing a uniform magnetic field over the entire sample volume. RF pulses applied to the sample cyclically invert the nuclear spins of the target isotopes, thereby modulating the dipole-dipole interaction between the detector magnet and the net nuclear magnetic moment of the sample, at the former's mechanical resonance frequency. The resulting motion of the mechanical resonator is detected using a fiber-optic interferometer. The electronics driving the RF coil are capable of producing the desired complex pulse sequences, allowing both single and double resonance NMR experiments. The displacement of the resonator driven by cyclic inversion of the sample's nuclear magnetic moment is recorded using fiber-optic interferometry. A "double" Fourier Transform process is subsequently employed to derive the NMR spectrum from the acquired data. A significant strength of the FDNMR technique over the conventional technique is that it is capable of high-resolution, multi-nuclear analysis [123]. It has been shown previously [122] that the force detection technique is uniquely suited for MEMS sizes and has superior sensitivity over the conventional, inductive detection technique for sample sizes in the range of 10–100 microns. Thus, the MEMS FDNMR spectrometer is the only choice for in-line detection of aqueous samples, as well as dissolved organic samples, in a miniaturized, multi-instrument suite type application.

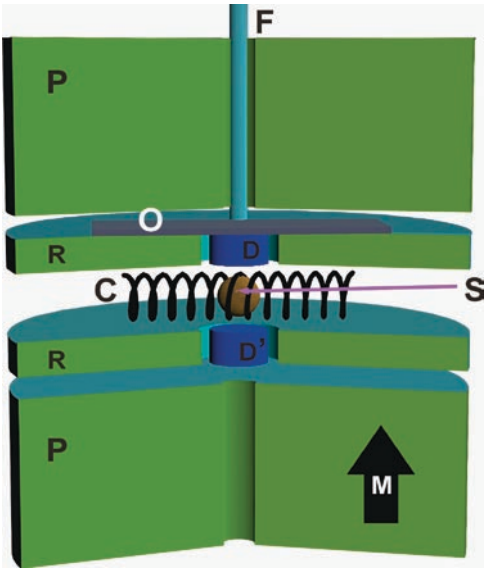

Fig. 13.17 Working principle of the MEMS-based FDNMR spectrometer. The sample (S) sits within an RF excitation coil (C), which modulates the NMR signal at the mechanical resonance frequency of a resonator made up of the detector magnet (D) and silicon beam (O). The detector magnet sits within an annular magnet (R) and the entire assembly is within the pole piece of an external field magnet (M). Detector magnet motion is measured using a fiber optic interferometer (F)

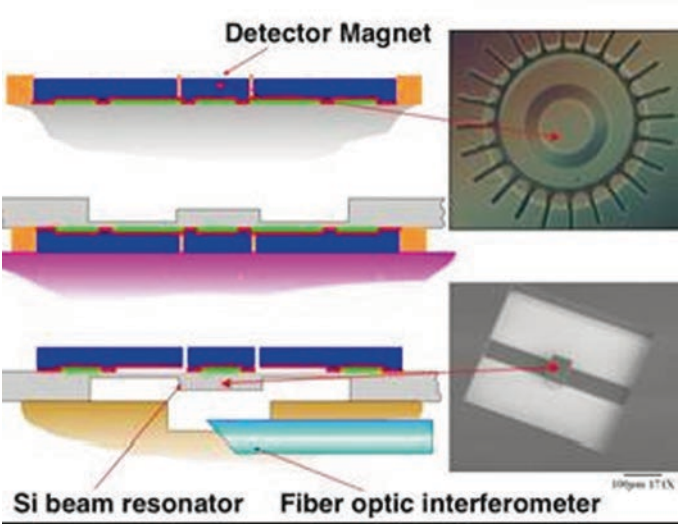

Fig. 13.18 Simplified processs schematic showing the major steps for fabrication and assembly of the MEMS FDNMR spectrometer. The steps involve electropating of a thin-film, multi-component, soft magnet alloy, fabrication of the Si beam resonator, and the final assembly of the spectrometer. Shown to the right are an optical micrograph of the electroplated 60 μm detector magnet, and an SEM image of the 400-μm-long Si beam resonator fabricated using Deep Reactive Ion Etching

In order to achieve the highest possible resolution for the NMR spectroscopy, it is important that the applied magnetic field be as high as possible. Our research determined that it is possible to electroplate a ternary, soft magnetic alloy of Fe–Ni–Co that is capable of producing a saturated, magnetic field of over 2 Tesla. The challenge lies in developing an electroplating process for a 10-μm-thick film with low stress, good morphology, and compositional uniformity. In addition, a precision lithography process was developed to produce thin-walled (1 μm), high aspect ratio (10:1) sacrificial layer "molds" for electroplating the soft magnet film.

13.5.2 NEMS Example: Nanogap Devices

Nanogaps have attracted attention as a means to contact individual molecules or nanocrystals for generating novel NEMS devices as well as for fundamental characterization studies [124]. Highly-controlled electrochemical nanogap fabrication with sub-angstrom precision has been successfully demonstrated using a gap-impedance-tuning mechanism (Fig. 13.19) [125]. Metal is deposited simultaneously on microfabricated electrodes separated by a several micron-sized gap. The deposition is conducted using a very low frequency feedback signal to monitor the electron tunneling current across the gap as it narrows. The current exhibits a stepwise increase when the gap is below 10 nm and subsequently an exponential increase in

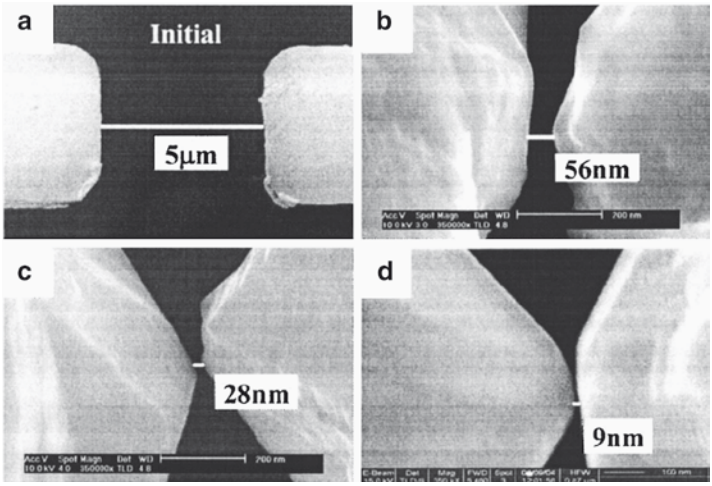

Fig. 13.19 SEM images of the gap electrodes: (**a**) the initial electrode pairs with the spacing of 5 mm fabricated by conventional photolithography; (**b**) the nanogap with a separation of 56 nm obtained at an ac sources frequency $f = 260$ Hz and the series resistances $R_1 = R_2 = 0.1$ kV; (**c**) the nanogap with a separation of 28 nm obtained at $f = 260$ Hz and $R_1 = R_2 = 1$ kV; (**d**) the nanogap with a separation of 9 nm at $f = 820$ Hz and $R_1 = R_2 = 1$ kV. Reprinted with permission from ref. [125]. Copyright 2005, American Institute of Physics

the tunneling current regime, corresponding to a gap size below 1 nm. The high level of precise control achieved by this fabrication technique allows for molecular manipulation of the nanogap [126, 127]. A key drawback of this technique is that although it is very efficient at producing angstrom size gaps, the precision in gap control falls sharply outside of the ~1 nm width required for the onset of electron tunneling. An alternative method uses one of the electrodes as a reference to detect the sharp potential drop when the electrical double layer is formed. This feedback enhancement has extended the generation of precisely controlled gaps to widths in the range of 10 nm [128]. Using a high frequency impedance feedback system similar to Tao et al, Liu et al have also demonstrated nanometer-level precision in controlling gaps in the range of 1–30 nm [129].

13.5.3 NEMS Example: Nanowire Barcodes

Keating and co-workers first investigated the use of segmented nanowires (nanowire "barcodes") for the detection of proteins and DNA using a sandwich immunoassay detection system [130]. The barcode nanowires consisted of alternating segments of Ag, Au, Ni, and Pt, with the Au segments functionalized with either specific nucleotide sequences for DNA detection or antibodies for protein detection. The lengths of the functionalized segments were also varied and alternated for creating the unique "barcodes" corresponding to specific proteins or oligonucleotides. Following exposure to the target analytes, the nanowire barcodes were introduced to the corresponding fluorophore-labeled markers, i.e. either complementary nucleotide sequences or antibodies.

The specificity of the detection scheme was demonstrated by correlating optical images of the nanowire barcodes acquired with and without fluorescence excitation. In this manner, multiple "probes" could be used simultaneously for the detection of a diverse set of analytes.

13.5.4 NEMS Example: Spintronics

Potential applications of ferromagnetic (e.g. nickel, cobalt, and permalloy) nanowires in high density magnetic recording and magnetoelectronics devices have attracted significant interest in understanding their magnetotransport properties [131–143]. Because of the extremely small dimensions and difficulties in addressing single nanowires, magnetotransport properties of nanowires have been mainly studied by measurements made on either lithographically fabricated ferromagnetic nanowire arrays [131, 134, 135, 139] or bundles of nanowires embedded within a suitable template [132, 136, 138, 140, 141]. Recently, Myung and coworkers [113, 114] have developed a facile technique for producing functional ferromagnetic devices based on single nanowires. This was achieved by a combination of processes.

Good electrical contacts for individual ferromagnetic nanowires were obtained by combining template-based electrodeposition techniques, with magnetic assembly, followed by post-annealing in a chemically reducing environment. The above fabrication and assembly technique allowed Myung et al to investigate the magnetotransport properties of single nanowires without interference from dipolar interactions between multiple nanowires. The magnetotransport properties of single electrodeposited ferromagnetic nanowires have been studied not only for nanowires with homogenous chemical composition but also for multi-segmented nanowires consisting of alternating lengths of ferromagnetic and nonmagnetic materials (e.g. NiFe/Cu, Ni/Cu, and Co/Cu). Measurements were aimed at characterizing the current-perpendicular-to-plane-giant-magnetoresistance (CPP-GMR) for these single nanowires [144–146]. Early results show that this approach requires additional work to overcome challenges that essentially limit reproducibility and high throughput. Problems notwithstanding, the approach shows great promise as a powerful platform to study the influence of different materials, dimensions, and structures (segmented, superlattice, and core/shell), on the magnetotransport properties of single nanowires that are crucial for developing a comprehensive knowledge base for spintronics applications.

13.5.5 NEMS Example: Nano Sensor

A diverse set of sensor devices including resistive elements and field effect transistors for chemical and biological detection have been fabricated using either top down or bottom up electrochemical synthesis. Equally diverse electrochemical fabrication methods have been used to generate these sensors, including ESED [95, 147], electrochemically coated CNT networks [97], template-free nanowires [103, 104], e-beam directed in-situ growth [39, 41, 42], and nanowire arrays [148]. In particular, high density nanowire arrays have gained attention because of their potential to detect multiple analytes within a compact and low mass device. Nanowires offer significant benefits over thin films in solid state sensor applications that exploit conductance changes in metals and metal oxides in the presence of gas analytes. Because of their significantly higher surface-to-volume ratio, nanowire-based devices have faster responses, lower power consumption, and higher sensitivities than their thin film counterparts. The large surface area to volume ratio enhances surface reactions and adsorption processes, driving the vastly improved properties of nanowire sensors. This is particularly true for biosensor applications in which antigens and proteins can be covalently attached to metal oxide nanowires using succinimidyl or carboxyl acid linkages [110, 149]. Zhou and coworkers have demonstrated biosensor systems binding prostate specific antigen antibodies (PSA-AB) to indium oxide nanowires via 3-phosphonopropionic linkages, and to single walled carbon nanotubes via 1-pyrenebutanoic acid succinimidyl ester groups (Fig. 13.20). Thiol groups, which are known to form self assembled monolayers (SAMs) on Au, can also facilitate the attachment of bio-molecules to Au nanowires with high binding affinities. Biocompatible conducting polymers can

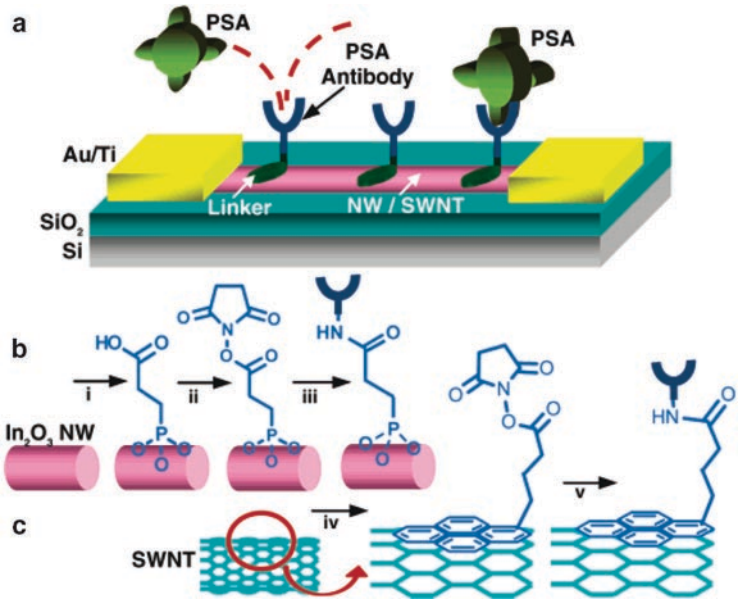

Fig. 13.20 (**a**) Schematic diagram of the nanosensor. PSA–ABs are anchored to the NW/SWNT surface and function as specific recognition groups for PSA binding. (**b**) Reaction sequence for the modification of In2O3 NW: *i*, deposition of 3-phosphonopropionic acid; *ii*, DCC and *N*-hydroxysuccinimide activation; *iii*, PSA-AB incubation. (**c**) Reaction sequence for the modification of SWNT: *i*V, deposition of 1-pyrenebutanoic acid succinimidyl ester; V, PSA-AB incubation. Reprinted with permission from ref. [149]. Copyright (2005) American Chemical Society

be functionalized through entrapment during electrodeposition [42], molecular imprinting [51, 52], and via covalent attachment to monomer precursors. These sensing schemes have the potential to satisfy the need for robust and easy-to-use diagnostic biomedical sensors by significantly reducing the time and complexity of bioassays. They provide a platform for label-free, real-time monitoring, resulting from the highly sensitive charge accumulation or depletion processes within the one-dimensional structures [150]. The sensitivity, selectivity, and rapid response for nanowire-based biosensors have been conclusively demonstrated by Zhou and coworkers for the detection of PSA (Fig. 13.21).

13.5.6 NEMS Example: Thermoelectric Devices

Thermoelectric materials have been used extensively for thermal sensing, energy conversion (heat to electricity), and for cooling (Peltier effect). In general, thermoelectric devices consist of n-type and p-type semiconductor constituents connected electrically in series and thermally in parallel [151]. While energy conversion efficiencies for thermoelectric devices are not yet competitive with conventional refrigerator or power generation systems, it is possible to achieve enhanced efficiencies

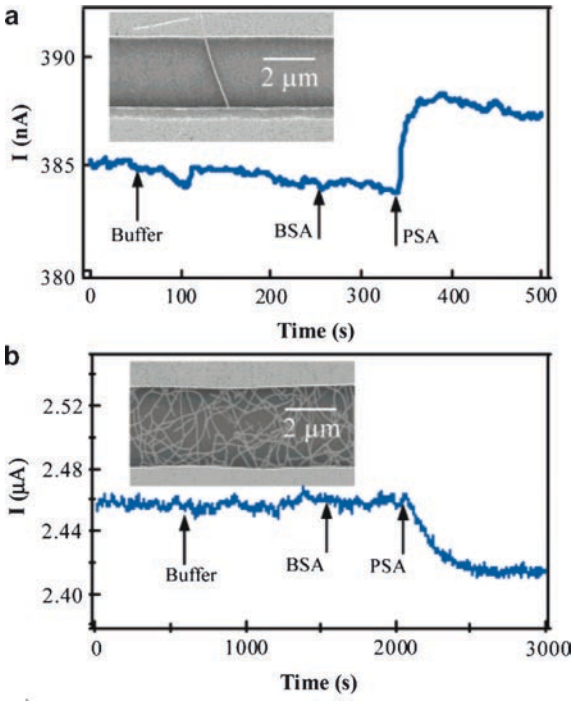

Fig. 13.21 Current recorded over time for an individual In2O3 NW device (**a**) and a SWNT mat device (**b**) when sequentially exposed to buffer, BSA, and PSA. Insets: SEM images of respective devices. Reprinted with permission from ref. [149]. Copyright (2005) American Chemical Society

through choices of novel materials and improved geometries. In particular, the nanowire geometry is particularly amenable to increase carrier mobility and decreased phonon transport arising from quantum confinement effects at the nanometer scale [152]. The key limitation standing in the way of achieving the promise of improved performance by thermoelectric nanowires is the ability to fabricate and couple together alternating n-type and p-type thermoelectric elements with high precision. Previous efforts at MEMS (micron) scales have successfully demonstrated thermoelectric microdevices containing over 100 electrochemically deposited Bi_2Te_3 (n-type) and Sb_2Te_3 (p-type) elements, each 60 μm in diameter, and fabricated using a LiGA technique [151]. This electrochemistry- based fabrication technique is highly scalable and inexpensive; however, the dimensions are still several orders of magnitude greater than the ideal dimensions (~10 nm) required to observe quantum confinement effects. While template based synthesis can certainly produce thermoelectric nanowires in this dimensional range, the key difficulty lies in ensuring that adjacent pores have alternating n-type and p-type semiconductor materials. In an effort to circumvent this problem, several researchers have used lithography to produce microzones of n-type and p-type nanowires and couple them to create the thermoelectric devices as shown in Fig. 13.22 [153, 154].

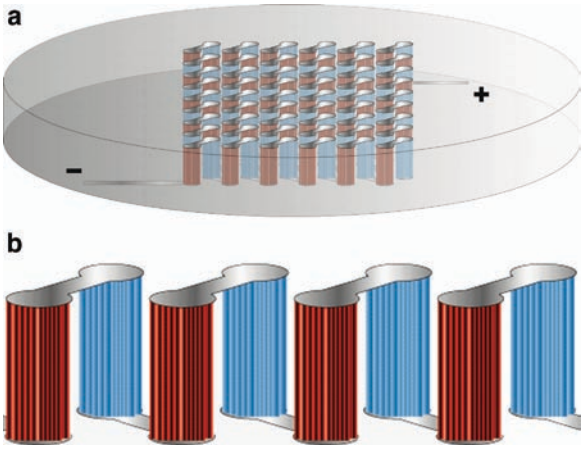

Fig. 13.22 (**a**) Proposed thermoelectric nanowire-based device within an alumina nanotemplate. (**b**) enlarged view of a few n-type and p-type nano-bundle elements connected electrically in series and arranged thermally in parallel (nanotemplate removed). Reprinted with permission from ref. [153]

13.6 Future Trends

Electrochemistry has gained recognition within the MEMS and NEMS community as an economical, high throughput means of producing a diverse range of materials and structures. As our understanding and requirements of materials have progressed, electrochemistry has grown to meet these demands, with tailored alloys, novel composites, and nanostructured features. However, considerable work remains to be done to adapt this centuries-old technology to the stringent demands of MEMS and NEMS. Specifically, a strong theoretical foundation resulting in robust modeling schemes for mass transport, current distribution, additive kinetics, and deposit nucleation needs to be developed in support of the largely empirical work in electrochemistry-based microfabrication that has been carried out thus far [6]. Beyond the actual fabrication process itself, considerable effort is required for developing an in-depth understanding of key electrodeposited materials properties including mechanical stress and interfacial adhesion, thermal, electrical, and chemical properties, all of which have a direct impact on the performance of MEMS and NEMS devices.

References

1. Mehragany M (1993) Microelectromechanical systems. IEEE Cuicuits Dev 8755–3996:14–22
2. Craighead HG (2000) Nanoelectromechanical systems. Science 290:1532–1535
3. Judy JW (2001) Microelectromechanical systems (MEMS): fabrication, design and application. Smart Mater Struct 10:1115–1134

4. Shacham-Diamand Y, Sverdlov Y (2000) Electrochemically deposited thin film alloys for ULSI and MEMS applications. Microelectron Eng 50:525–531
5. Peeters E (1997) Challenges in commercializing MEMS. IEEE Comput Sci Eng 4:44–48
6. Datta M, Landolt D (2000) Fundamental aspects and applications of electrochemical microfabrication. Electrochim Acta 45:2535–2558
7. Osaka T (2000) Electrodeposition of highly functional thin films for magnetic recording devices of the next century. Electrochim Acta 45:3311–3321
8. Vereecken PM, Binstead RA, Delgianni H, Andricacos PC (2005) The chemistry of additives in damascene copper plating. IBM J Res Dev 49:3–18
9. Moffat TP, Wheeler D, Edelstein MD, Josell D (2005) Superconformal film growth: mechanism and quantification. IBM J Res Dev 49:19–36
10. Myung NV, Park DY, Yoo BY, Sumodjo PTA (2003) Development of electroplated magnetic materials for MEMS. J Magn Magn Mater 265:189–198
11. Andricacos PC, Robertson N (1998) Future directions in electroplated materials for thin-film recording heads. IBM J Res Dev 42:671–680
12. Guan S, Nelson BJ (2005) Electrodeposition o f low residual stress CoNiMnP hard magnetic thin films for magnetic MEMs actuators. J Magn Magn Mater 292:49–58
13. Agarwala R, Agarwala V (2003) Electroles alloy/composite coatings: a review. Sadhana 28:475–493
14. Gawrilov GG (1979) Chemical (electroless) nickel plating, 1st edn. Portcullis Press Limited, Redhill
15. Khoperia TN, Tabatadze TJ, Zedgenidze TI (1997) Formation of microcircuits in microelectronics by electroless deposition. Electrochim Acta 42:3049–3055
16. Chen CJ, Lin KL (2000) Internal stress and adhesion of amorphous Ni–Cu–P alloy on aluminum. Thin Solid Films 370:106–113
17. Hsu JC, Lin KL (2003) Enhancement in the deposition behavior and deposit properties of electroless Ni–Cu–P. J Electrochem Soc 150:C653–C656
18. Osaka T (2004) Creation of highly functional thin films using electrochemical nanotechnology. Chem Rec 4:346–362
19. Shacham-Diamand Y, Inberg A, Sverdlov Y, Bogush V, Croitoru N, Moscovich H, Freeman A (2003) Electroless processes for micro- and nanoelectronics. Electrochim Acta 48:2987–2996
20. Sun L, Chien C-L, Searson PC (2004) Fabrication of nanoporous nickel by electrochemical dealloying. Chem Mater 16:3125–3129
21. Guell AG, Diez-Perez I, Gorostiza P, Sanz F (2004) Preparation of reliable probes for electrochemical tunneling spectroscopy. Anal Chem 76:5218–5222
22. West AC, Deligianni H, Andricacos PC (2005) Electrochemical planarization of interconnect metallization. IBM J Res Dev 49:37–48
23. Datta M (1995) Fabrication of an array of precision nozzles by through-mask electrochemical micromachining. J Electrochem Soc 142:3801–3805
24. Schuster R, Kirchner V, Allongue P, Ertl G (2000) Electrochemical micromachining. Science 289:98–101
25. Shaw KA, Zhang ZL, MacDonald NC (1994) SCREAM I: a single mask, single-crystal silicon, reactive ion etching process for microelectromechanical structures. Sens Actuators 40:63–70
26. Guckel H (1998) High-aspect-ratio micromachining via deep x-ray lithography. Proc IEEE 86:1586
27. Madou MJ (2002) Fundamentals of microfabrication, 2nd edn. CRC Press LLC, Boca Raton
28. Griffiths SK (2004) Fundamental limitations of LIGA x-ray lithography: sidewall onset, slope and minimum feature size. J Micromech Microeng 14:999–1011
29. Griffiths SK, Crowell JA, Kistler BL, Dryden AS (2004) Dimensional errors in LIGA-produced metal structures due to thermal expansion and swelling of PMMA. J Micromech Microeng 14:1548–1557
30. Goods SH, Kelly JJ, Yang NYC (2004) Electrodeposited nickel-manganese: an alloy for microsystem applications. Microsyst Technol Micro Nanosyst Inf Storage Process Syst 10:498–505

31. Kelly JJ, Goods SH, Yang NYC (2003) High performance nanostructured Ni–Mn alloy for microsystem applications. Electrochem Solid State Lett 6:C88–C91
32. Marquis EA, Talin AA, Kelly JJ, Goods SH, Michael JR (2006) Effects of current density on the structure of Ni and Ni–Mn electrodeposits. J Appl Electrochem 36:669–676
33. Yang JM, Zhu D, Qu NS, Lei WN (2004) Pulse electroforming of nanocrystalline Ni–Mn alloy. Adv Grinding Abrasive Process 259–2:596–601
34. Cohen A, Zhang G, Tseng F-G, Frodis U, Mansfeld F, Will F (1999) EFAB: rapid, low-cost desktop micromachining of high aspect ratio True 3-D MEMS. In: Twelfth IEEE international conference on micro electro mechanical systems, 1999. MEMS '99, pp 244–251
35. Chen R (2004) Micro-Fabrication Techniques. Wireless Des Develop 16–20
36. Malek CK, Saile V (2004) Applications of LIGA technology to precision manufacturing of high-aspect-ratio micro-components and -systems: a review. Microelectronics J 35:131–143
37. Alper SE, Ocak IE, Akin T (2006) Ultra-thick and high-aspect-ratio nickel microgyroscope using EFAB™ multi-layer additive electroforming. In: 19th IEEE international conference on micro electro mechanical systems, 2006. MEMS 2006 Istanbul, pp 670–673
38. Microfabrica (2004) Going beyond silicon MEMS with EFAB technology. pp 1–14
39. Yun M, Myung NV, Vasquez RP, Lee C, Menke E, Penner RM (2004) Electrochemically grown wires for individually addressable sensor arrays. Nano Lett 4:419–422
40. Ramanathan K, Bangar MA, Chen MYW, Mulchandani A, Myung NV (2004) Individually addressable conducting polymer nanowires array. Nano Lett 4:1237–1239
41. Im Y, Lee C, Vasquez RP, Bangar MA, Myung NV, Menke EJ, Penner RM, Yun M (2006) Investigation of a single Pd nanowire fo use as a hydrogen sensor. Small 2:356–358
42. Ramanathan K, Bangar MA, Yun M, Chen W, Myung NV, Mulchandani A (2005) Bioaffinity sensing using biologically functionalized conducting-polymer nanowire. J Am Chem Soc 127:496–497
43. Peng C-Y, Kalkan AK, Fonash SJ, Bu B, Sen A (2005) A "Grow-in-Place" architecture and methodology for electrochemical synthesis of conducting polymer nanoribbon device arrays. Nano Lett 5:439–444
44. Brumlik CJ, Martin CR (1991) Template synthesis of metal microtubules. J Am Chem Soc 113:3174–3175
45. Martin CR (1995) Nanomaterials: a membrane-based synthetic approach. Science 266:1961–1966
46. Martin CR (1995) Template synthesis of electronically conductive polymer nanostructures. Acc Chem Res 28:61–68
47. He H, Tao NJ (2003) Electrochemical fabrication of metal nanowires. In: Nalwa HS (ed) Encyclopedia of nanoscience and nanotechnology, vol X. American Scientific Publishers, pp 1–18
48. Kovtyukhova NI, Martin BR, Mbindyo JKN, Mallouk TE, Cabassi M, Mayer TS (2002) Layer-by-layer self-assembly strategy for template synthesis of nanoscale devices. Mater Sci Eng C 19:255–262
49. Kovtyukhova NI, Martin BR, Mbindyo JKN, Smith PA, Razavi B, Mayer TS, Mallouk TE (2001) Layer-by-layer assembly of rectifying junctions in and on metal nanowires. J Phys Chem B 105:8762–8769
50. Xu X, Chen L, Wang C, Yao Q, Feng C (2005) Template synthesis of heterostructured polyaniline/Bi_2Te_3 nanowires. J Solid State Chem 178:2163–2166
51. Li Y, Yang HH, You QH, Zhuang ZX, Wang XR (2006) Protein recognition via surface molecularly imprinted polymer nanowires. Anal Chem 78:317–320
52. Li Y, Yin X-F, Chen F-R, Yang H-H, Zhuang Z-X, Wang Z-R (2006) Synthesis of magnetic molecularly imprinted polymer nanowires using a nanoporous alumina template. Macromolecules 39:4497–4499
53. Park S, Chung SW, Mirkin CA (2004) Hybrid organic-inorganic, rod-shaped nanoresistors and diodes. J Am Chem Soc 126:11772–11773
54. Kovtyukhova NI, Kelley BK, Mallouk TE (2004) Coaxially gated in-wire thin-film transistors made by template assembly. J Am Chem Soc 126:12738–12739

55. Keller F, Hunter MS, Robinson DL (1953) Structural features of oxide coatings on aluminum. J Electrochem Soc 100:411–419
56. Huczko A (2000) Template-based synthesis of nanomaterials. Appl Phys A 70:365–376
57. Nielsch K, Choi J, Schwirn K, Wehrspohn RB, Gosele U (2002) Self-ordering regimes of porous alumina: the 10% porosity rule. Nano Lett 2:677–680
58. Xu T, Zangari G, Metzger RM (2002) Periodic holes with 10 nm diameter produced by grazing Ar^+ milling of the barrier layer in hexagonally ordered nanoporous alumina. Nano Lett 2:37–41
59. Masuda H, Hasegwa F, Ono S (1997) Self-ordering of cell arrangement of anodic porous alumina formed in sulfuric acid solution. J Electrochem Soc 144:L127–L130
60. Masuda H, Satoh M (1996) Fabrication of gold nanodot array using anodic porous alumina as an evaporation mask. Jpn J Appl Phys 35:L126–L129
61. Masuda H, Yamada J, Satoh M, Asoh J (1997) Highly ordered nanochannel-array architecture in anodic alumina. Appl Phys Lett 71:2770–2772
62. Yoo BY, Hendricks RK, Ozkan M, Myung NV (2006) Three-dimensional alumina nanotemplate. Electrochim Acta 51:3543–3550
63. Jee SE, Lee PS, Yoon B-J, Jeong S-H, Lee K-H (2005) Fabrication of microstructures by wet etching of anodic aluminum oxide substrates. Chem Mater 17:4049–4052
64. Cojocaru CS, Padovani JM, Wade T, Mandoli C, Jaskierowicz G, Wegrowe JE, AFi M, Pribat D (2005) Conformal anodic oxidation of aluminum thin films. Nano Lett 5:675–680
65. Chien CL, Sun L, Tanase M, Bauer LA, Hultgren A, Silevitch DM, Meyer GJ, Searson PC, Reich DH (2002) Electrodeposited magnetic nanowires: arrays, field-induced assembly, and surface functionalization. J Magn Magn Mater 249:146–155
66. Sun L, Searson PC, Chien CL (1999) Electrochemical deposition of nickel nanowire arrays in single-crystal mica films. Appl Phys Lett 74:2803–2805
67. Schonenberger C, vanderzande BMI, Fokkink LGJ, Henny M, Schmid C, Kruger M, Bachtold A, Huber R, Birk H, Staufer U (1997) Template synthesis of nanowires in porous polycarbonate membranes: electrochemistry and morphology. J Phys Chem B 101:5497–5505
68. Williams WD, Giordano N (1984) Fabrication of 80-a metal wires. Rev Sci Instrum 55:410–412
69. Brinker CJ, Lu Y, Sellinger A, Fan H (1999) Evaporation-induced self-assembly nanostructures made easy. Adv Mater 11:579–585
70. Lu Y, Fan H, Stump A, Ward TL, Rieker T, Brinker J (1999) Aerosol-assisted self-assembly of mesostructured sphereical nanoparticles. Nature 398:223–226
71. Lu Y, Gangull R, Drewien CA, Anderson MT, Brinker CJ, Gong W, Guo Y, Soyez H, Dunn B, Huang MH, Zink JI (1997) Continuous formation of supported cubic and hexagonal mesoporous films by sol-gel dip-coating. Nature 389:364–368
72. Lu Y, Yang H, Sellinger A, Lu M, Huang J, Fan H, Haddad R, Lopez G, Burns AR, Sasaki DY, Shelnutt J, Brinker CJ (2001) Self-assembly of mesoscopically ordered chromatic polydiacetylene/silica nanocomposites. Nature 410:913–917
73. Wang D, Luo H, Kou R, Gil MP, Xiao S, Golub VO, Yang Z, Brinker CJ, Lu Y (2004) A general route to macroscopic hierarchical 3D nanowire networks. Angew Chem Int Ed 43:6169–6173
74. Wang D, Zhou WL, McCaughy BF, Hampsey JE, Ji Z, Jiang Y-B, HuifangXu TJ, Schmehl RH, O'Connor C, Brinker CJ, Lu Y (2003) Electrodeposition of metallic nanowire thin films using mesoporous silica templates. Adv Mater 15:130–133
75. Morkved TL, Lu M, Urbas AM, Ehrichs EE, Jaeger HM, Mansky P, Russell TP (1996) Local control of microdomain orientation in diblock copolymer thin films with electric fields. Science 273:931–933
76. Xu T, Hawker CJ, Russell TP (2005) Interfacial interaction dependence of microdomain orientation in diblock copolymer thin films. Macromolecules 38:2802–2805
77. Kim SO, Solak HH, Stoykovich MP, Ferrier NJ, de Pablo JJ, Nealey PF (2003) Epitaxial self-assembly of block copolymers on lithographically defined nanopatterned substrates. Nature 424:411–414

78. Xu T, Zvelindovsky AV, Sevink GJA, Lyakhova KS, Jinnai H, Russell TP (2005) Electric field alignment of asymmetric diblock copolymer thin films. Macromolecules 38:10788–10798
79. Xu T, Goldbach JT, Leiston-Belanger J, Russell TP (2004) Effect of ionic impurities on the electric field alignment of diblock copolymer thin films. Colloid Polym Sci 282:927–931
80. Thurn-Albrecht T, Schotter J, Kastle GA, Emley N, Shibauchi T, Krusin-Elbaum L, Guarini K, Black CT, Tuominen MT, Russell TP (2000) Ultrahigh-density nanowire arrays grown in self-assembled diblock copolymer templates. Science 290:2126–2129
81. Lopes WA, Jaeger HM (2001) Hierarchical self-assembly of metal nanostructures on diblock copolymer scaffolds. Nature 414:735–738
82. Allred DB, Sarikaya M, Baneyx F, Schwartz DT (2005) Electrochemical nanofabrication using crystalline protein masks. Nano Lett 5:609–613
83. Dai HX, Choe WS, Thai CK, Sarikaya M, Traxler BA, Baneyx F, Schwartz DT (2005) Nonequilibrium synthesis and assembly of hybrid inorganic-protein nanostructures using an engineered DNA binding protein. J Am Chem Soc 127:15637–15643
84. Dai HX, Thai CK, Sarikaya M, Baneyx F, Schwartz DT (2004) Through-mask anodic patterning of copper surfaces and film stability in biological media. Langmuir 20:3483–3486
85. Thai CK, Dai HX, Sastry MSR, Sarikaya M, Schwartz DT, Baneyx F (2004) Identification and characterization of Cu2O- and ZnO-binding polypeptides by Escherichia coli cell surface display: toward an understanding of metal oxide binding. Biotechnol Bioeng 87:129–137
86. Li QG, Penner RM (2005) Photoconductive cadmium sulfide hemicylindrical shell nanowire ensembles. Nano Lett 5:1720–1725
87. Menke EJ, Li Q, Penner RM (2004) Bismuth telluride (Bi2Te3) nanowires synthesized by cyclic electrodeposition/stripping coupled with step edge decoration. Nano Lett 4:2009–2014
88. Walter EC, Murray BJ, Favier F, Kaltenpoth G, Grunze M, Penner RM (2002) Noble and coinage metal nanowires by electrochemical step edge decoration. J Phys Chem B 106: 11407–11411
89. Walter EC, Murray BJ, Favier F, Penner RM (2003) "Beaded" bimetallic nanowires: wiring nanoparticles of metal 1 using nanowires of metal 2. Adv Mater 15:396–399
90. Zach MP, Ng KH, Penner RM (2000) Molybdenum nanowires by electrodeposition. Science 290:2120–2123
91. Banks CE, Davies TJ, Wildgoose GG, Compton RG (2005) Electrocatalysis at graphite and carbon nanotube modified electrodes: edge-plane sites and tube ends are the reactive sites. Chem Commun 7:829–841
92. Fan YW, Goldsmith BR, Collins PG (2005) Identifying and counting point defects in carbon nanotubes. Nat Mater 4:906–911
93. Walter EC, Zach MP, Favier F, Murray BJ, Inazu K, Hemminger JC, Penner RM (2003) Metal nanowire arrays by electrodeposition. Chemphyschem 4:131–138
94. Zach MP, Inazu K, Ng KH, Hemminger JC, Penner RM (2002) Synthesis of molybdenum nanowires with millimeter-scale lengths using electrochemical step edge decoration. Chem Mater 14:3206–3216
95. Favier F, Walter EC, Zach MP, Benter T, Penner RM (2001) Hydrogen sensors and switches from electrodeposited palladium mesowire arrays. Science 293:2227–2231
96. Fennimore AM, Yuzvinsky TD, Han WQ, Fuhrer MS, Cumings J, Zettl A (2003) Rotational actuators based on carbon nanotubes. Nature 424:408–410
97. Chen XH, Chen CS, Xiao HN, Liu HB, Zhou LP, Li SL, Zhang G (2006) Dry friction and wear characteristics of nickel/carbon nanotube electroless composite deposits. Tribol Int 39:22–28
98. Kong J, Chapline MG, Dai HJ (2001) Functionalized carbon nanotubes for molecular hydrogen sensors. Adv Mater 13:1384–1386
99. Day TM, Unwin PR, Wilson NR, Macpherson JV (2005) Electrochemical templating of metal nanoparticles and nanowires on single-walled carbon nanotube networks. J Am Chem Soc 127:10639–10647

100. Huang JX, Kaner RB (2004) A general chemical route to polyaniline nanofibers. J Am Chem Soc 126:851–855
101. Huang JX, Virji S, Weiller BH, Kaner RB (2003) Polyaniline nanofibers: facile synthesis and chemical sensors. J Am Chem Soc 125:314–315
102. Liang L, Liu J, Windisch CF, Exarhos GJ, Lin YH (2002) Direct assembly of large arrays of oriented conducting polymer nanowires. Angew Chem Int Ed 41:3665–3668
103. Wang J, Chan S, Carlson RR, Luo Y, Ge GL, Ries RS, Heath JR, Tseng HR (2004) Electrochemically fabricated polyaniline nanoframework electrode junctions that function as resistive sensors. Nano Lett 4:1693–1697
104. Alam MM, Wang J, Guo YY, Lee SP, Tseng HR (2005) Electrolyte-gated transistors based on conducting polymer nanowire junction arrays. J Phys Chem B 109:12777–12784
105. Jin S, Whang DM, McAlpine MC, Friedman RS, Wu Y, Lieber CM (2004) Scalable interconnection and integration of nanowire devices without registration. Nano Lett 4:915–919
106. Tao A, Kim F, Hess C, Goldberger J, He RR, Sun YG, Xia YN, Yang PD (2003) Langmuir-Blodgett silver nanowire monolayers for molecular sensing using surface-enhanced Raman spectroscopy. Nano Lett 3:1229–1233
107. Whang D, Jin S, Lieber CM (2003) Nanolithography using hierarchically assembled nanowire masks. Nano Lett 3:951–954
108. Whang D, Jin S, Wu Y, Lieber CM (2003) Large-scale hierarchical organization of nanowire arrays for integrated nanosystems. Nano Lett 3:1255–1259
109. Yang PD, Kim F (2002) Langmuir-Blodgett assembly of one-dimensional nanostructures. Chemphyschem 3:503–506
110. Tanase M, Bauer LA, Hultgren A, Silevitch DM, Sun L, Reich DH, Searson PC, Meyer GJ (2001) Magnetic alignment of fluorescent nanowires. Nano Lett 1:155–158
111. Tanase M, Silevitch DM, Hultgren A, Bauer LA, Searson PC, Meyer GJ, Reich DH (2002) Magnetic trapping and self-assembly of multicomponent nanowires. J Appl Phys 91:8549–8551
112. Bentley AK, Trethewey JS, Ellis AB, Crone WC (2004) Magnetic manipulation of copper-tin nanowires capped with nickel ends. Nano Lett 4:487–490
113. Hangarter CM, Myung NV (2005) Magnetic alignment of nanowires. Chem Mater 17:1320–1324
114. Yoo B, Rheem Y, Beyermann WP, Myung NV (2006) Magnetically assembled 30 nm diameter nickel nanowire with ferromagnetic electrodes. Nanotechnology 17:2512–2517
115. Niyogi S, Hangarter C, Thamankar RM, Chiang YF, Kawakami R, Myung NV, Haddon RC (2004) Magnetically assembled multiwalled carbon nanotubes on ferromagnetic contacts. J Phys Chem B 108:19818–19824
116. Duan XF, Huang Y, Cui Y, Wang JF, Lieber CM (2001) Indium phosphide nanowires as building blocks for nanoscale electronic and optoelectronic devices. Nature 409:66–69
117. Smith PA, Nordquist CD, Jackson TN, Mayer TS, Martin BR, Mbindyo J, Mallouk TE (2000) Electric-field assisted assembly and alignment of metallic nanowires. Appl Phys Lett 77:1399–1401
118. Yamamoto K, Akita S, Nakayama Y (1998) Orientation and purification of carbon nanotubes using ac electrophoresis. J Phys D Appl Phys 31:L34–L36
119. Dong LF, Bush J, Chirayos V, Solanki R, Jiao J (2005) Dielectrophoretically controlled fabrication of single-crystal nickel silicide nanowire interconnects. Nano Lett 5:2112–2115
120. Edwards B, Mayer TS, Bhiladvala RB (2006) Synchronous electrorotation of nanowires in fluid. Nano Lett 6:626–632
121. Fan DL, Zhu FQ, Cammarata RC, Chien CL (2005) Controllable high-speed rotation of nanowires. Phys Rev Lett 94:247208
122. George T, Madsen L, Tang W, Chang-Chien A, Leskowitz G, Weitekamp D (2001) MEMS-based force-detected nuclear magnetic resonance spectrometer for in situ planetary exploration. In: IEEE, pp 273–278
123. Leskowitz GM, Madsen LA, Weitekamp DP (1998) Force-detected magnetic resonance without field gradients. Solid State Nucl Magn Reson 11:73–86

124. Xu BQ, Tao NJJ (2003) Measurement of single-molecule resistance by repeated formation of molecular junctions. Science 301:1221–1223
125. Chen F, Qing Q, Ren L, Wu ZY, Liu ZF (2005) Electrochemical approach for fabricating nanogap electrodes with well controllable separation. Appl Phys Lett 86:123105
126. Li CZ, He HX, Tao NJ (2000) Quantized tunneling current in the metallic nanogaps formed by electrodeposition and etching. Appl Phys Lett 77:3995–3997
127. Li CZ, Tao NJ (1998) Quantum transport in metallic nanowires fabricated by electrochemical deposition/dissolution. Appl Phys Lett 72:894–896
128. Liu B, Xiang J, Tian JH, Zhong C, Mao BW, Yang FZ, Chen ZB, Wu ST, Tian ZQ (2005) Controllable nanogap fabrication on microchip by chronopotentiometry. Electrochim Acta 50:3041–3047
129. Qing Q, Chen F, Li PG, Tang WH, Wu ZY, Liu ZF (2005) Finely tuning metallic nanogap size with electrodeposition by utilizing high-frequency impedance in feedback. Angew Chem Int Ed 44:7771–7775
130. Nicewarner-Pena SR, Freeman RG, Reiss BD, He L, Pena DJ, Walton ID, Cromer R, Keating CD, Natan MJ (2001) Submicrometer metallic barcodes. Science 294:137–141
131. Goolaup S, Singh N, Adeyeye AO, Ng V, Jalil MBA (2005) Transition from coherent rotation to curling mode reversal process in ferromagnetic nanowires. Eur Phys J B 44:259–264
132. Hao Z, Shaoguang Y, Gang N, Dongliang Y, Youwei D (2001) Study on magnetic property of Fe14Ni86 alloy nanowire array. J Magn Magn Mater 234:454–458
133. Lederman M, O'Barr R, Schultz S (1995) Experimental study of individual ferromagnetic sub-micron cylinders. IEEE Trans Magn 31:3793–3795
134. Leven B, Dumpich G (2005) Resistance behavior and magnetization reversal analysis of individual Co nanowires. Phys Rev B 71:064411(7 pages)
135. Martin JI, Velez M, Alameda JM, Briones F, Vicent JL (2002) Magnetotransport properties of patterned magnetic Ni wires of submicrometric dimensions. J Magn Magn Mater 240:14–16
136. Navas D, Asenjo A, Jaafar M, Pirota KR, Hernandez-Velez M, Sanz R, Lee W, Niesch K, Batallan F, Vazquez M (2005) Magnetic behavior of NixFe(100-x) (65 <= x <= 100) nanowire arrays. J Magn Magn Mater 290:191–194
137. OBarr R, Schultz S (1997) Switching field studies of individual single domain Ni columns. J Appl Phys 81:5458–5460
138. Ohgai T, Gravier L, Hoffer X, Lindeberg M, Hjort K, Spohr R, Ansermet J-P (2003) Template synthesis and magnetoresistance property of Ni and Co single nanowires electrodeposited into nanopores with a wide range of aspect ratios. J Phys D Appl Phys 36:3109–3114
139. Perez-Junquera A, Martin JI, Velez M, Alameda JM, Vicent JL (2003) Temperature dependence of the magnetization reversal process in patterned Ni nanowires. Nanotechnology 14:294–298
140. Pignard S, Goglio G, Radulescu A, Piraux L, Dubois S, Declemy A, Duvail JL (2000) Study of the magnetization reversal in individual nickel nanowires. J Appl Phys 87:824–829
141. Wegrowe JE, Gilbert SE, Kelly D, Doudin B, Ansermet JP (1998) Anisotropic magnetoresistance as a probe of magnetization reversal in individual nano-sized nickel wires. IEEE Trans Magn 34:903–905
142. Wegrowe JE, Kelly D, Franck A, Gilbert SE, Ansermet JP (1999) Magnetoresistance of ferromagnetic nanowires. Phys Rev Lett 82:3681–3684
143. Wernsdorfer W, Doudin B, Mailly D, Hasselbach K, Benoit A, Meier J, Ansermet JP, Barbara B (1996) Nucleation of magnetization reversal in individual nanosized nickel wires. Phys Rev Lett 77:1873–1876
144. Chen M, Searson PC, Chien CL (2003) Micromagnetic behavior of electrodeposited Ni/Cu multilayer nanowires. J Appl Phys 93:8253–8255
145. Dubois S, Marchal C, Beuken JM, Piraux L, Duvail JL, Fert A, George JM, Maurice JL (1997) Perpendicular giant magnetoresistance of NiFe/Cu multilayered nanowires. Appl Phys Lett 70:396–398

146. Evans PR, Yi G, Schwarzacher W (2000) Current perpendicular to plane giant magnetoresistance of multilayered nanowires electrodeposited in anodic aluminum oxide membranes. Appl Phys Lett 76:481–483
147. Murray BJ, Walter EC, Penner RM (2004) Amine vapor sensing with silver mesowires. Nano Lett 4:665–670
148. Kolmakov A, Zhang YX, Cheng GS, Moskovits M (2003) Detection of CO and O-2 using tin oxide nanowire sensors. Adv Mater 15:997–1000
149. Li C, Curreli M, Lin H, Lei B, Ishikawa FN, Datar R, Cote RJ, Thompson ME, Zhou CW (2005) Complementary detection of prostate-specific antigen using ln(2)O(3) nanowires and carbon nanotubes. J Am Chem Soc 127:12484–12485
150. Wanekaya AK, Chen W, Myung NV, Mulchandani A (2006) Nanowire-based electrochemical biosensors. Electroanalysis 18:533–550
151. Snyder GJ, Lim JR, Huang CK, Fleurial JP (2003) Thermoelectric microdevice fabricated by a MEMS-like electrochemical process. Nat Mater 2:528–531
152. Hicks LD, Dresselhaus MS (1993) Thermoelectric figure of merit of a one-dimensional conductor. Phys Rev B 47:16631–16634
153. Lim JR, Whitacre JF, Fleurial JP, Huang CK, Ryan MA, Myung NV (2005) Fabrication method for thermoelectric nanodevices. Adv Mater 17:1488–1492
154. Wang W, Jia FL, Huang QH, Zhang JZ (2005) A new type of low power thermoelectric micro-generator fabricated by nanowire array thermoelectric material. Microelectron Eng 77:223–229
155. Kim SH, Misner MJ, Xu T, Kimura M, Russell TP (2004) Highly oriented and ordered arrays from block copolymers via solvent evaporation. Adv Mater 16:226–231
156. George T (2003) Overview of MEMS/NEMS technology development for space applications at NASA/JPL. SPIE 5116:136–148
157. Possin GE (1970) A method of forming very small diameter wires. Rev Sci Instrum 41:772–774
158. Luo, H, Wang D, He J, Lu Y (2005) Magnetic cobalt nanowire thin films. J Phys Chem B 109:1919–1922
159. Klein JD, Herrick RD, Palmer D, Sailor MJ, Brumlik CJ, Martin CR (1993) Electrochemical fabrication of cadmium chalcogenide microdiode arrays. Chem Mater 5:902–904
160. Sima M, Enculescu I, Visan T (2004) The electrodeposition of semiconductor nanowires with thermoelectric properties using “template” method. Revista De Chimie 55:743–746
161. Mukherjee PK, Chakravorty D (2004) Growth of CdS nanowires using Na-4 mica as template. J Appl Phys 95:3164–3169
162. Wang DH, Jakobson HP, Kou R, Tang J, Fineman RZ, Yu DH, Lu YF (2006) Metal and semiconductor nanowire network thin films with hierarchical pore structures. Chem Mater 18:4231–4237
163. Li Y, Meng GW, Zhang LD, Phillipp F (2000) Ordered semiconductor ZnO nanowire arrays and their photoluminescence properties. App Phy Lett 76:2011–2013